

# A NASA GISTEMPv4 Observational Uncertainty Ensemble

Nathan Lenssen<sup>1,2</sup>, Gavin A. Schmidt<sup>3</sup>, Michael Hendrickson<sup>3,6</sup>, Peter Jacobs<sup>4</sup>,  
Matthew J. Menne<sup>5</sup>, Reto Ruedy<sup>3,6</sup>

<sup>1</sup>Dept. of Earth and Environmental Sciences, Columbia University, New York, New York, USA

<sup>2</sup>Dept. of Applied Mathematics and Statistics, Colorado School of Mines, Golden, Colorado, USA

<sup>3</sup>NASA Goddard Institute for Space Studies, New York, New York, USA

<sup>4</sup>NASA Goddard Space Flight Center, Greenbelt, Maryland, USA

<sup>5</sup>NOAA National Centers for Environmental Information, Asheville, North Carolina, USA

<sup>6</sup>Autonomic Integra LLC, New York, New York, USA

## Key Points:

- A 200-member ensemble quantifies uncertainty in historical surface temperature anomalies as estimated by GISTEMP
- This ensemble enables accurate statistical analyses of key global change metrics such as trends and rankings of temperature records.
- The median ensemble estimate agrees with the operational GISTEMP analyses and other global products

## Abstract

The historical global temperature record is an essential data product for quantifying the variability and change of the Earth system. In recent years, better characterization of observational uncertainty in global and hemispheric trends has become available, but the methodologies are not necessarily applicable to analyses at smaller regional areas, or monthly or seasonal means, where station sparsity and other systematic issues contribute to greater uncertainty. This study presents a gridded uncertainty ensemble of historical surface temperature anomalies from the Goddard Institute for Space Studies (GISS) Surface Temperature (GISTEMP) product. This ensemble characterizes the complex spatial and temporal correlation structure of uncertainty, enabling better uncertainty propagation for climate and applied science at regional and sub-annual scales. This work details the methodology for generating the uncertainty ensemble, presents key statistics of the uncertainty evolution over space and time, and provides best practices for using the uncertainty ensemble in future studies. Summary statistics from the uncertainty ensemble agree with the previous GISTEMP global uncertainty assessment, providing confidence in both.

## 1 Introduction

In recent years, better characterization of uncertainty in observed global and hemispheric temperature trends has become available (Lenssen et al., 2019; Morice et al., 2020; Huang et al., 2020; Rohde & Hausfather, 2020), but the methodologies are not necessarily applicable to smaller spatiotemporal scales such as regional or monthly averages, where station sparsity and other systematic issues contribute to greater uncertainty. This study describes an ensemble of temperature reconstructions for the Goddard Institute for Space Studies (GISS) Surface Temperature product (GISTEMP) product (Hansen et al., 2010; Lenssen et al., 2019) which spans the possible regional and monthly uncertainty while properly accounting for the underlying spatiotemporal correlation structure.

Previous work quantified uncertainty in the GISTEMP estimate of large-scale annual mean series and developed critical components necessary for quantifying the uncertainty in the GISTEMP historical surface temperature record (Lenssen et al., 2019). Critically, Lenssen et al. (2019) formalized the various sources of uncertainty in the GISTEMP procedure and divided total uncertainty into independent, quantifiable components that represented the major sources of uncertainty in the land and ocean analyses. In the Land Surface Air Temperature (LSAT) record, the primary sources of uncertainty are sampling

50 uncertainty and station homogenization uncertainty. Sampling uncertainty is an umbrella  
51 term for uncertainties introduced into global and regional means due to incomplete spatial  
52 and temporal coverage. Station homogenization uncertainty accounts for possible errors  
53 arising from the adjustment of single station records to correct artificial break points due  
54 to changes in observing methods or station locations. Using this framework, operational  
55 GISTEMP now provides an estimate of global mean uncertainty.

56 Extending the results of Lenssen et al. (2019) to regional and monthly mean tempera-  
57 ture is a significant undertaking. There are two primary difficulties: (1) moving from global  
58 and large-scale spatial means to small-scale spatial means and (2) quantifying the temporal  
59 dependence of the uncertainty to provide accurate estimates of the uncertainty in changes  
60 in the mean. The temporal structure of the uncertainty is the most important problem,  
61 and is particularly important to capture correctly for accurate uncertainty quantification  
62 in global and regional trends. The simple 95% confidence intervals for the global mean  
63 discussed in Lenssen et al. (2019) do not include information about the temporal structure  
64 of uncertainty. It is well known that significant temporal autocorrelation in uncertainty  
65 exists, primarily driven over the land surface by the homogenization of the station record  
66 (Menne et al., 2018). The temporal structure of this homogenization uncertainty is highly  
67 persistent and not well represented by common statistical models for time series such as  
68 auto-regressive or more complex ARIMA models.

69 Creating ensembles of equally likely realizations of the global temperature record is  
70 the current best practice for quantifying and presenting uncertainty in gridded monthly  
71 historical temperature analyses (Morice et al., 2012, 2020; Huang et al., 2020). The Hadley  
72 Centre with HadCRUT4 (Morice et al., 2012) and HadCRUT5 (Morice et al., 2020) as well  
73 as NOAA’s GlobalTemp Version 5 (Huang et al., 2020) have shifted their global tempera-  
74 ture uncertainty products from simple confidence intervals to such uncertainty ensembles.  
75 In addition, the newer deep neural network (DNN)-based infilling of HadCRUT5 by the  
76 German Climate Computation Center (DKRZ), or the DKRZ-DNN global product, uses  
77 the HadCRUT5 ensemble to quantify uncertainty in their infilling method (Kadow et al.,  
78 2020). Each of these ensembles represent the complex and persistent temporal structure of  
79 the uncertainties inherent in the global temperature record, enable more accurate estimates  
80 of uncertainty in global and regional temperature change, and make it straightforward to  
81 include observational uncertainty in subsequent analyses.

82 This study presents a monthly, gridded GISTEMPv4 uncertainty ensemble from 1880-  
83 2020. Following the operational GISTEMP analysis, Land Surface Air Temperature (LSAT)  
84 is calculated from station records from NOAA NCEI’s Global Historical Climatology Net-  
85 work (GHCN) monthly version 4 (GHCNm v4; (Menne et al., 2018)). Sea Surface Tempera-  
86 ture (SST) data from NOAA’s Extended Reconstructed Sea Surface Temperature version 5  
87 (ERSSTv5; (Huang et al., 2017)) is merged with the LSAT analysis to form the GISTEMP  
88 global land-ocean analysis (Hansen et al., 2010; Lenssen et al., 2019).

89 One of the primary motivations behind the GISTEMP uncertainty ensemble is to  
90 increase the awareness of observational uncertainty in studies relying on historical tempera-  
91 ture data. The global historical temperature record, and GISTEMP in particular, is widely  
92 accessed, cited, and used in subsequent studies: From the 10-most cited papers that cite  
93 Lenssen et al. (2019), direct applications of GISTEMP include: the validation of historical  
94 runs of global general circulation models (Swart et al., 2019; Held et al., 2019; Danabasoglu  
95 et al., 2020; Notz & SIMIP Community, 2020), retrospectively evaluating past climate model  
96 projections (Hausfather et al., 2020), verifying estimates of climate sensitivity (Tokarska et  
97 al., 2020), quantifying changes in mean climate and extremes over the historical period  
98 (Myhre et al., 2019), and estimating the cost of carbon emission in the global economy  
99 (Carleton et al., 2020). Despite the scientific and societal importance of the problems ad-  
100 dressed in these studies, and their reliance on the historical global temperature record, none  
101 of them include observational uncertainty as part of their methodologies.

102 A potential reason for the near ubiquitous omission of observational uncertainty in  
103 analyses involving historical climate data is the lack of accessible, interpretable, and easily-  
104 implemented uncertainty products. Observational ensembles are a large step forward, as  
105 posterior distributions of a key result in an analysis that relies on historical temperature  
106 can be constructed nearly trivially by running the analysis of interest on each uncertainty  
107 ensemble member. However, these ensembles are relatively new, only appearing in the  
108 last decade, with very few studies utilizing them as yet. Thus, this study also includes a  
109 description of easy-to-implement best practices for including observational uncertainty in  
110 studies that use historical surface temperature products.

111 The remainder of this paper is organized as follows. Section 2 outlines the source data  
112 used for the analyses. Section 3 provides a brief background on the LSAT uncertainty model  
113 discussed in detail in (Lenssen et al., 2019). Section 4 presents the methods used to generate

114 the GISTEMP uncertainty ensemble. Section 5 summarizes the statistical properties of the  
115 GISTEMP uncertainty ensemble. Section 6 discusses the implications of the results and  
116 provides best practices for implementing the GISTEMP uncertainty ensemble in future  
117 studies.

## 118 **2 Input Data**

### 119 **2.1 LSAT Data: GHCNm Version 4**

120 The GHCNm version 4 dataset is a quality-controlled collection of station-based land  
121 temperature records at the monthly temporal resolution (Menne et al., 2018). All station  
122 records included in the dataset are processed to correct for irregularities arising due to  
123 change of station location, measurement method, and surrounding land cover. In addition to  
124 a single authoritative station record, GHCNm v4 also contains a 100+ member uncertainty  
125 ensemble that spans the parametric uncertainty arising from choices in the homogenization  
126 procedure as detailed in Menne et al. (2018). This study uses the GHCNm v4 ensemble to  
127 capture the station and bias uncertainties as is discussed further in Section 3.

### 128 **2.2 SST Data: ERSSTv5**

129 The latest version of NOAA’s gridded sea surface temperature analysis, ERSSTv5, is  
130 used to quantify the historical monthly SST anomalies globally (Huang et al., 2017). The  
131 product is distributed on a  $2^\circ \times 2^\circ$  grid that is interpolated to the 8000 GISTEMP equal area  
132 boxes to be compatible with the operational GISTEMP python analysis. The uncertainty  
133 quantification in ERSSTv4/v5 breaks down ocean uncertainty into parametric uncertainty,  
134 or uncertainty arising from choices the ERSST method, and reconstruction uncertainty, or  
135 uncertainty arising from estimating global SST from limited SST records. The ERSSTv5  
136 uncertainty model contains small updates to the parameters from the ERSSTv4 uncertainty  
137 method, but is otherwise identical (Liu et al., 2015; Huang et al., 2016, 2017). ERSSTv5  
138 provides a 1,000 member uncertainty ensemble of gridded SST fields as well as a 500 member  
139 operational uncertainty ensemble, enabling other operational products to take advantage of  
140 their uncertainty assessment.

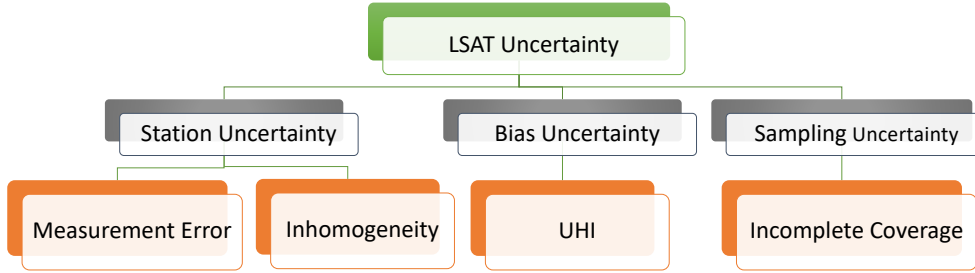


**Figure 1.** Decomposition the total LSAT uncertainty into the three major categories and the most common sources. The connections on the chart denote dependence, implying statistical independence between cells that are not connected.

### 141 2.3 ERA5 Reanalysis

142 This study uses the monthly ECMWF Reanalysis version 5 (ERA5) from 1951-2020  
 143 as an approximate, full-coverage historical LSAT record (Hersbach et al., 2020). The 2 m  
 144 temperature field is averaged to the final  $2^\circ \times 2^\circ$  GISTEMP uncertainty ensemble grid to  
 145 facilitate direct comparison between ERA5 and GISTEMP. ERA5 is chosen as the reanalysis  
 146 as a it best replicates the observed global mean over its period (Lenssen et al., 2019; Hersbach  
 147 et al., 2020). As shown in Lenssen et al. (2019), global and large-scale GISTEMP uncertainty  
 148 estimates derived from ERA5 agree with the JRA-55 and MERRA2 reanalyses.

## 149 3 LSAT Uncertainty

150 There are three major, statistically independent, categories of uncertainty that arise  
 151 in the LSAT record (Figure 1). A brief introduction to these uncertainties is provided  
 152 though see Morice et al. (2012), and Lenssen et al. (2019) for more details. The uncertainty  
 153 ensemble model accounts for station and bias uncertainties through the GHCNm v4 ensemble  
 154 as detailed in Section 4.1 and sampling uncertainties following the methodology outlined in  
 155 Section 4.2.

156 Station uncertainty arises from errors in the temperature record of a single station.  
 157 The first sources of station uncertainty are instrumental errors from limited thermometer  
 158 precision. These are relatively small and uncorrelated in space and time, making them  
 159 essentially a non-issue for monthly records (Morice et al., 2012). The other and more  
 160 significant sources of station uncertainty are inhomogeneities, or non-climatic shifts in mean

161 in station records. These can arise from local microclimate shifts or changes in the station  
162 measurement method. As mentioned in Section 2.1, the GHCNm dataset attempts to detect  
163 and correct for these inhomogeneities, but this is a difficult problem, and uncertainty due  
164 to statistical estimation of these corrections adds uncertainty to estimates of regional and  
165 global temperature while reducing any bias (e.g. (Hausfather et al., 2013)).

166 Bias uncertainty refers to anthropogenic changes in local climate that are not repre-  
167 sentative of changes in the regional or global climate system. Generally, this category of  
168 uncertainty refers to the enhanced warming observed in cities commonly referred to as the  
169 urban heat island (UHI) effect. Again, the GHCNm dataset accounts for these, but correc-  
170 tions add uncertainty to the surface temperature record. This issue has also been tackled  
171 in GISTEMP through the use of nightlights to characterize the more urban environments  
172 (Hansen et al., 2010).

173 Sampling uncertainty arises from estimating regional and global temperature due to  
174 limited spatial and temporal coverage. The distribution of the global observation network  
175 does not fully cover the land surface and has changed over time. GISTEMP uses the spatial  
176 correlation of temperature anomalies to increase the coverage (Hansen et al., 2010; Cowtan  
177 et al., 2018). By interpolating the station-level anomalies, GISTEMP is able to make a  
178 more accurate estimate of the global temperature, but at a cost of introducing uncertainty  
179 into fine-scale regional means.

180 Due to the different sources and relative contributions of these uncertainties, represent-  
181 ing uncertainty at each location and month as independent or correlated Gaussian random  
182 variables is an incomplete method. In particular, uncertainty arising due to errors in the  
183 homogenization process have long-term persistence that are not well-suited to ARIMA time  
184 series models. Construction of an LSAT uncertainty ensemble using an iterative process  
185 where each step accounts for one of the two major categories of uncertainty, is better able to  
186 better represent the spatiotemporal structure of the uncertainties, and can be understood  
187 in isolation.

## 188 4 Methods

### 189 4.1 GHCN-ERSST-GISTEMP Ensemble

190 The core of the GISTEMP uncertainty is the GHCN-ERSST-GISTEMP ensemble  
191 which is generated by running 100 potential station records from the GHCNm v4 uncertainty

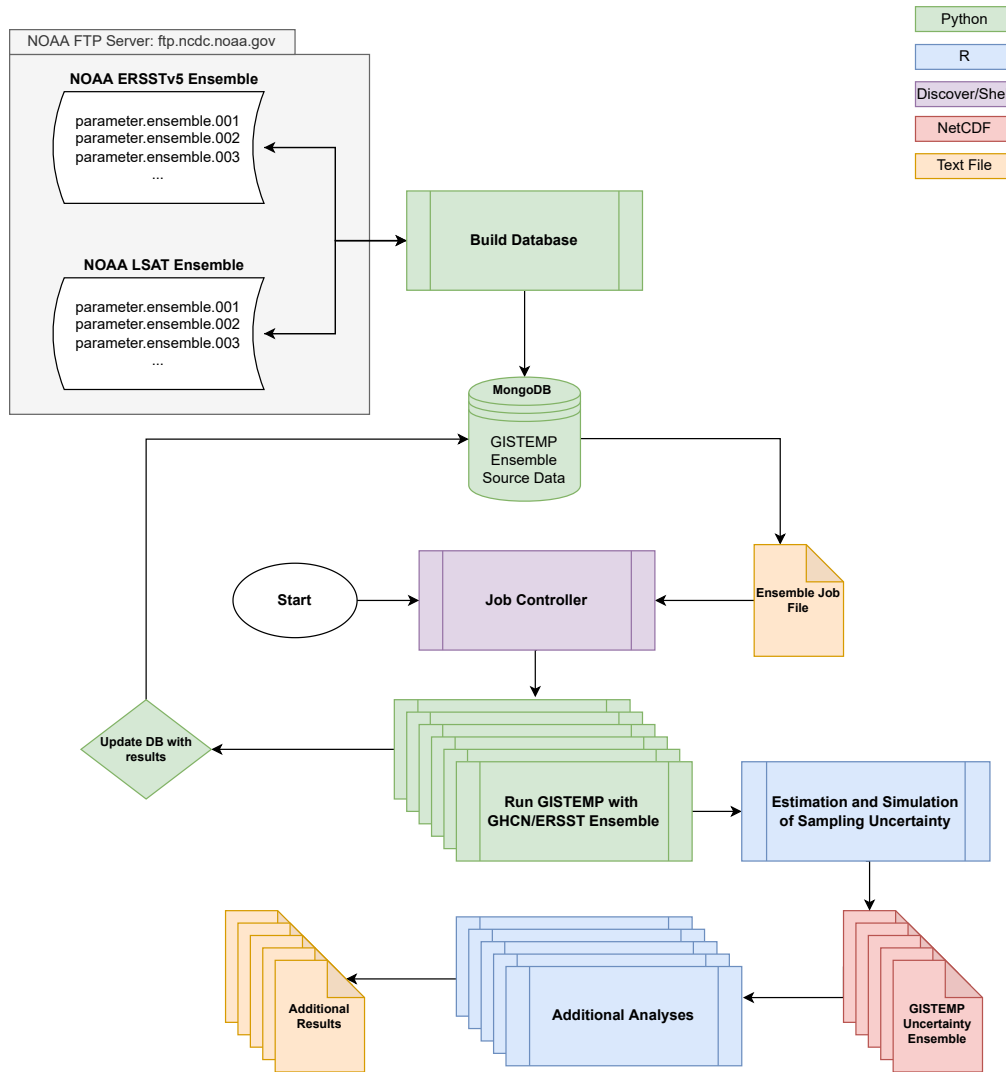


**Figure 2.** Organization of the analysis from the raw NOAA data in the upper-left corner to the final country-level mean estimates in the bottom-left corner. The legend in the upper-right denotes the primary language or datatype of each node.

192 paired with 100 of the ERSSTv5 uncertainty ensemble members. These station record-ocean  
 193 record pairs are then run through the operational Python GISTEMP analysis code (Barnes  
 194 & Jones, 2011). This process is outlined visually in the code flowchart (Figure 2) through  
 195 steps at the top of the chart leading up to the block labeled “Run GISTEMP with NOAA  
 196 Ensemble Data.” The GHCN ensemble is 100 possible station records in the same format as  
 197 the version of GHCN used in production GISTEMP. Temperature fields and mean time series  
 198 are calculated as described in Chapter 1 (Hansen et al., 2010; Lenssen et al., 2019). The 100

199 member GHCN-ERSST-GISTEMP ensemble accounts for all quantified SST uncertainty as  
200 well as homogenization and bias LSAT uncertainty. Thus, all that remains is to quantify  
201 the LSAT sampling uncertainty arising from limited station coverage as detailed in Section  
202 4.2.

203 Managing the output of the ensemble members to ensure computations are working  
204 as intended and output is documented appropriately, is a critical part of the workflow.  
205 The steps in the flowchart prior to the “Run GISTEMP with GHCN/ERSST Ensemble”  
206 block describe the data and code management processes needed to organize the analysis  
207 on the NASA Center for Climate Simulations (NCCS) high performance cloud computing  
208 environment. By porting the analysis, the GHCN-ERSST-GISTEMP ensemble is able to be  
209 generated in under an hour as opposed to the days it would take to run on a typical laptop.

## 210 4.2 Sampling Uncertainty Ensemble

211 The 100 member GHCN-ERSST-GISTEMP ensemble detailed above in Section 4.1  
212 accounts for the station and bias uncertainties. To incorporate the sampling uncertainty,  
213 2 possible realizations of the sampling uncertainty are simulated and added to each of the  
214 100 members of the GHCN/GISTEMP, resulting in a final uncertainty ensemble of 200  
215 members. This step is performed in R (R Core Team, 2020) and is denoted by the blue  
216 “Estimation and Simulation of Sampling Uncertainty” on the analysis flowchart (Figure 2).

217 The sampling uncertainty is quantified using an improved version of GISTEMP sam-  
218 pling uncertainty analysis detailed in Lenssen et al. (2019). The ERA5 reanalysis from  
219 1950-2020 is used as an approximate historical climate with full global coverage. For each  
220 decade from 1880-2020, a proxy station record is created by masking full-field ERA5 record  
221 to match the station coverage for that decade. That is, a station mask is created for  
222 1880 – 1889, 1890 – 1899, . . . , 2000 – 2009, 2010 – 2020 where the last proxy station record  
223 includes 2020. Following Lenssen et al. (2019), a grid-cell is considered covered in a decade  
224 if it has a station with coverage for at least 5 of the 10 years. Annual coverage requires a  
225 station has coverage for at least 3 seasons which requires at least two months in the season.

226 The GISTEMP interpolation step with 1,200km smoothing is applied to the masked  
227 ERA5 data resulting in estimates of regional temperature on a  $2^\circ \times 2^\circ$  grid. The true  
228 temperature anomaly fields from ERA5 are differenced to calculate reconstruction error  
229 fields for each time-step in the ERA5 record. These reconstruction error fields are an

230 estimate of the uncertainty in the LSAT field due to limited station coverage as well as  
231 uncertainty introduced by the GISTEMP interpolation method.

232 Due to the interpolation in the GISTEMP method, the reconstruction error fields have  
233 spatial structure that must be accounted for. Here, the empirical reconstruction error fields  
234 are used as draws from the sampling uncertainty distribution as they inherently contain  
235 the correct spatial correlation structure. As the sampling uncertainty is independent to the  
236 homogenization uncertainty, the monthly empirical reconstruction error fields are added to  
237 each of the gridded GHCN-ERSST-GISTEMP ensemble members discussed in Section 4.1.

238 The sampling uncertainty also has temporal persistence due to autocorrelation in the  
239 monthly temperature anomaly fields. To conservatively account for this temporal persis-  
240 tence, a random block of length 1–12 months is selected from the empirical reconstruction  
241 error fields. This method is an extension of the 12 month persistence of uncertainty used in  
242 the HadCRUT5 method (Morice et al., 2020) which reduces artifacts in time series calcu-  
243 lated using the uncertainty ensemble. Note that the month of the empirical reconstruction  
244 error field is selected to align with the month of the GISTEMP ensemble as the underlying  
245 temperature variability and therefore uncertainty varies seasonally.

### 246 **4.3 Calculation of Global and Large-Scale Series Ensembles**

247 One would naively expect to be able to use the ensemble to calculate the magnitude of  
248 uncertainty in a time series such as the global annual mean by simply calculating the time  
249 series of interest in each of the 200 GISTEMP uncertainty ensemble members. However,  
250 this method does not account for the uncertainty in such series due to grid cells that do  
251 not have estimates. To include this uncertainty, an additional 200 member GISTEMP  
252 uncertainty ensemble is created that includes this uncertainty by modifying the sampling  
253 uncertainty step discussed above. As before, the empirical reconstruction error fields are  
254 added to the GHCN-ERSST-GISTEMP ensemble at each monthly time step for grid-cells  
255 where GISTEMP is making estimates. However, for grid-cells where GISTEMP does not  
256 make estimates due to limited station or ship coverage, the missing value is replaced with  
257 the “true” value from ERA5 from the same ERA5 time-step that was used for the empirical  
258 reconstruction error field. This method both includes the uncertainty added to large-scale  
259 series by not making temperature anomaly estimates at all locations in the interpolation  
260 step, as well as includes the correct spatial structure by ensuring this uncertainty comes

261 from the same underlying “true” temperature field that was used to estimate the sampling  
262 uncertainty.

263 This full-coverage uncertainty ensemble fully captures the uncertainty of global and  
264 other large scale means. The GISTEMP averaging procedure is applied to each of the  
265 200 members, resulting in a 200 member ensemble each of global, hemispheric, band, and  
266 land-only/ocean-only monthly and annual temperature series.

#### 267 **4.4 Decomposition of the LSAT Uncertainty**

268 The full-coverage GISTEMP uncertainty ensemble described in Section 4.3 also allows  
269 the decomposition of global annual LSAT uncertainty into sampling and homogenization  
270 for comparison with Figure 4 of Lenssen et al. (2019). The global annual LSAT homoge-  
271 nization uncertainty is calculated as the spread of the 200 members land-only global annual  
272 mean temperature anomaly from the GHCN-ERSST-GISTEMP, excluding any addition of  
273 sampling uncertainty. The global annual LSAT sampling uncertainty is calculated as the  
274 spread of 200 members simulated following the full-coverage GISTEMP sampling ensem-  
275 ble detailed above where empirical reconstruction error values are used when GISTEMP  
276 provides an estimate and ERA5 values of corresponding ERA5 time-steps are used when  
277 GISTEMP does not provide an estimate.

## 278 **5 Results and Discussion**

279 The global and hemispheric annual mean series are calculated with the GISTEMP  
280 uncertainty ensemble by applying the GISTEMP averaging scheme to each of the 200 gridded  
281 ensemble members. The ensemble median matches very well with operational GISTEMP for  
282 each of these series (Figure 3). The 95% confidence intervals of mean series are constructed as  
283 the empirical 95% confidence interval from the 200 annual mean series. The 95% confidence  
284 interval of the ensemble mean and hemispheric series covers the operational series at every  
285 time point, which along with the near-perfect agreement between the ensemble median and  
286 the operational series, validates the GISTEMP uncertainty ensemble’s ability to accurately  
287 replicate the global mean calculation.

288 The ensemble estimate of uncertainty in the global annual mean is uniformly lower  
289 than the analysis of Lenssen et al. (2019) (Figure 4). This could be due to either lower SST  
290 or LSAT uncertainty or a positive correlation between the SST and LSAT, assumed zero in

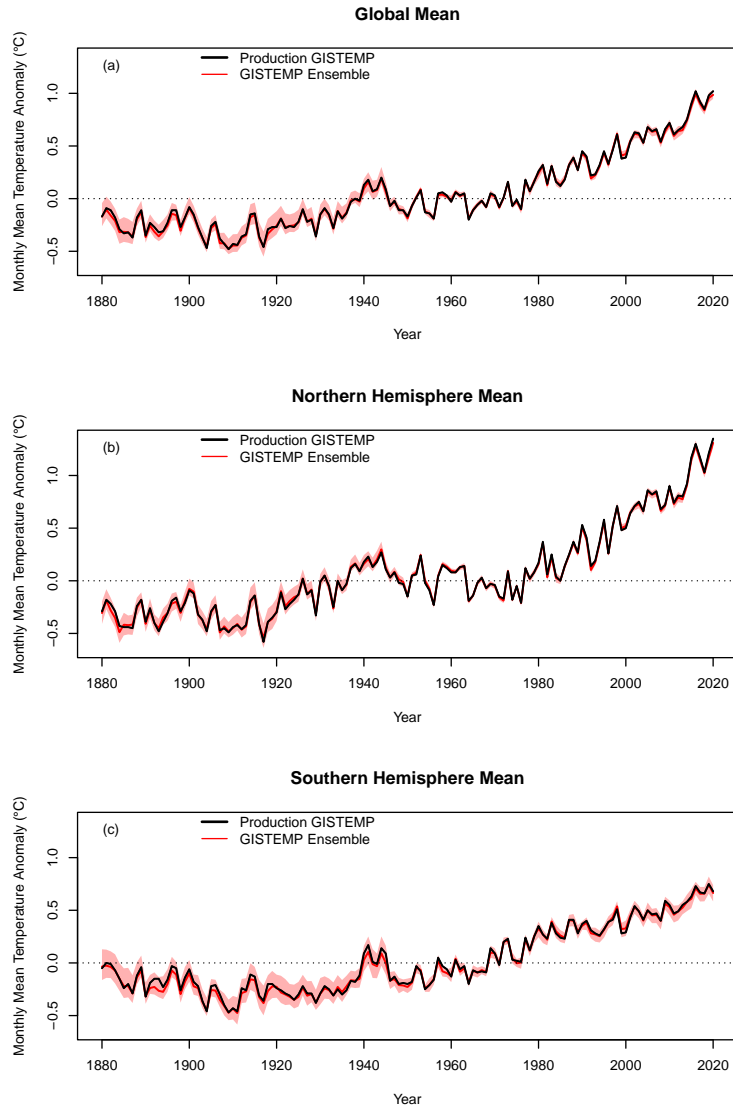


**Figure 3.** A comparison of the global and hemispheric annual mean series as calculated from operational GISTEMP and the GISTEMP ensemble. The solid red line is the median of the GISTEMP ensemble.

291 the Lenssen et al. (2019) analysis. The SST uncertainty is quantified by the same ERSSTv5  
 292 ensemble used in the first analysis and can't be the source of the discrepancy. Decompos-  
 293 ing the ensemble global annual land surface uncertainty into its two components suggests  
 294 that much smaller homogenization uncertainty is the primary reason for the smaller global  
 295 uncertainty estimate presented here (Figure 5). This is expected as the homogenization  
 296 uncertainty in the global mean in Lenssen et al. (2019) was quantified on a  $5^\circ \times 5^\circ$  grid, but  
 297 did not include any additional smoothing or corrections. However, the GISTEMP averaging

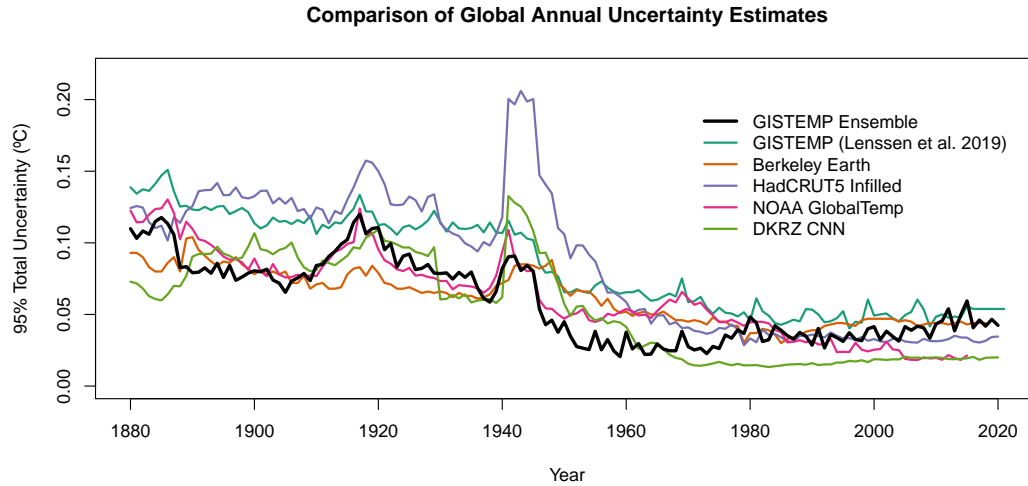


**Figure 4.** The global annual mean 95% confidence intervals for the new GISTEMP ensemble, the same calculation as performed in Lenssen et al. (2019), and the two products that publish operational confidence intervals.

298 method includes all station information within 1,200 km when estimating the temperature  
 299 anomaly of a gridbox as well as corrects all station records to account for mean-shift biases  
 300 by comparing nearby station records over complete time periods (Hansen & Lebedeff, 1987).  
 301 This additional homogenization step dramatically reduces the homogenization uncertainty,  
 302 particularly in the early part of the record.

303 The estimate of the uncertainty in the global annual mean temperature anomaly from  
 304 the GISTEMP ensemble is close to the other major global analyses that publish uncertainty  
 305 estimates (Figure 4): HadCRUT5 (Morice et al., 2020), NOAA GlobalTemp (Huang et al.,  
 306 2020), Berkeley Earth (Rohde & Hausfather, 2020), and DKRZ-DNN (Kadow et al., 2020).  
 307 The GISTEMP Ensemble estimate closely mirrors that of NOAA GlobalTemp as expected  
 308 due to the shared source data uncertainty quantification between the two products. The  
 309 largest deviation in products is the very large uncertainty in HadCRUT5 during the WWII  
 310 period in the early 1940s. This large uncertainty is a conservative estimate of the large biases  
 311 found in SST data during this period that have not yet been incorporated in operational  
 312 ship record databases (Chan et al., 2019).

313 The GISTEMP ensemble provides uncertainty at monthly temporal resolution, allow-  
 314 ing analyses of uncertainty in monthly mean temperature change. Monthly uncertainties

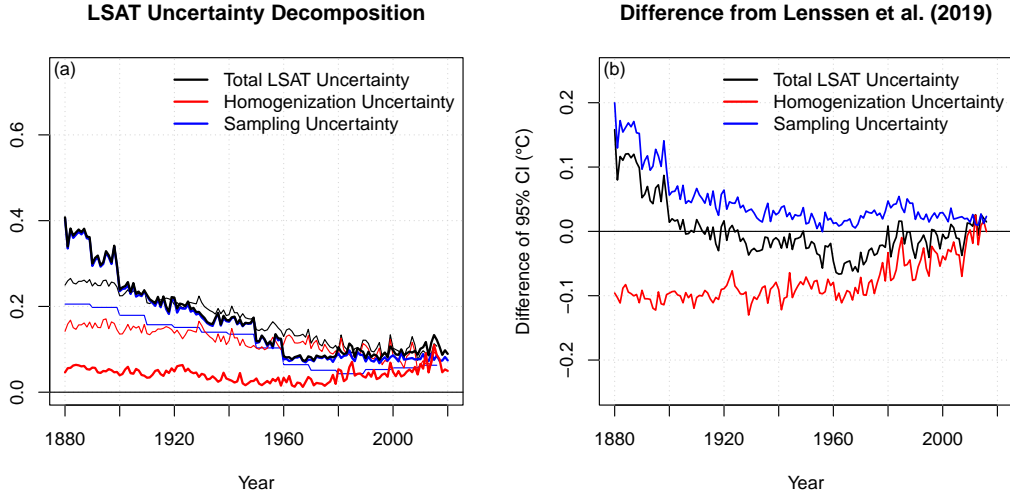


**Figure 5.** (a) The annual LSAT uncertainty ( $2\sigma$ ) decomposed into the sampling and homogenization uncertainty components. The dark lines show the calculation from the ensemble analysis and the thin lines show the Lenssen et al. (2019) calculation. (b) The difference of the LSAT uncertainties between the ensemble and the global analysis of Lenssen et al. (2019).

315 are slightly smaller in the NH winter ( $0.06^{\circ}\text{C}$ ) than the summer months ( $0.08^{\circ}\text{C}$ ), be-  
 316 cause of the greater uncertainty in SH winters – particularly in Antarctica which has the  
 317 worst coverage and largest homogenization uncertainty. We see that the uncertainty in the  
 318 January and July global mean temperature series is again much smaller than the warming  
 319 signal (Figure 6). Using the July 2020 uncertainty estimate as the approximate uncertainty  
 320 of the GISTEMP July 2023 anomaly of  $1.18^{\circ}\text{C}$ , we conclude that July 2023 is the warmest  
 321 global month on record with nearly 100 % certainty.

322 Decomposing the annual LSAT mean into the homogenization and sampling com-  
 323 ponents reveals that the LSAT uncertainty, at least globally, it dominated by sampling  
 324 uncertainty for the majority of the record (Figure 5). In the Lenssen et al. (2019), homog-  
 325 enization and sampling uncertainty in the global LSAT mean were calculated separately  
 326 and then combined assuming independence. However, it is shown here that the additional  
 327 homogenization done in GISTEMP when averaging multiple station records reduces homog-  
 328 enization uncertainty to levels substantially smaller than raw GHCN, at least at the global  
 329 scale.

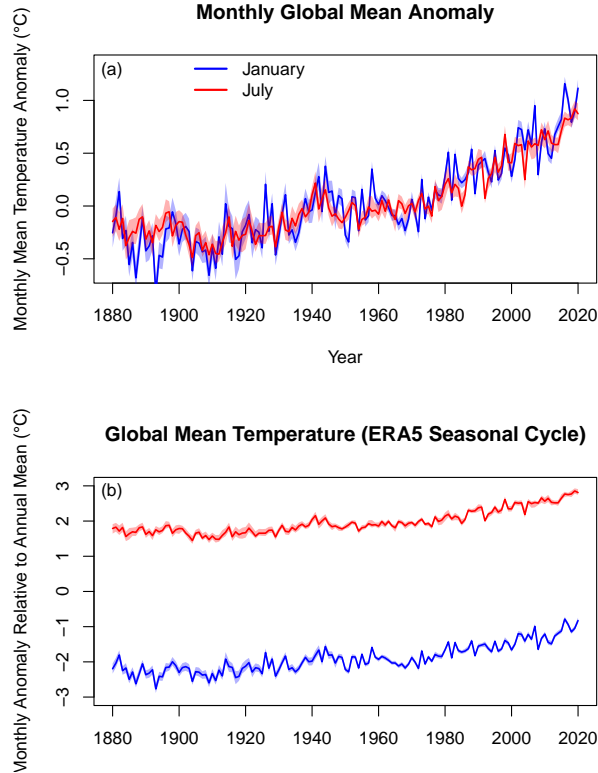


**Figure 6.** The global mean January and July time series and 95% confidence intervals for (a) the global mean temperature anomalies with respect to a 1950-1979 climatology and (b) the global mean anomaly scaled by the seasonal cycle using ERA5 to estimate the seasonal cycle of global temperature.

330 Sampling uncertainty is the dominant source of uncertainty for nearly the entire land  
 331 surface (Figure 7), in agreement with the global LSAT decomposition. The sampling un-  
 332 certainties are particularly dominant for regions with dense station coverage where homog-  
 333 enization uncertainties are nearly zero. The only area where homogenization uncertainty  
 334 dominates is the central Amazon and parts of Antarctica, both regions with known major  
 335 inhomogeneities and very few nearby station observations to use in correction methods.

336 Looking at the GISTEMP latitudinal band mean estimates from the uncertainty en-  
 337 semble, large uncertainty in the polar regions appears to be driving the global uncertainty  
 338 (Figure 8). This uncertainty is driven by land and sea ice regions near the poles (Figure  
 339 9). Again, there is very good agreement between the operational and ensemble GISTEMP  
 340 with the ensemble confidence interval always covering the operational series. In general, the

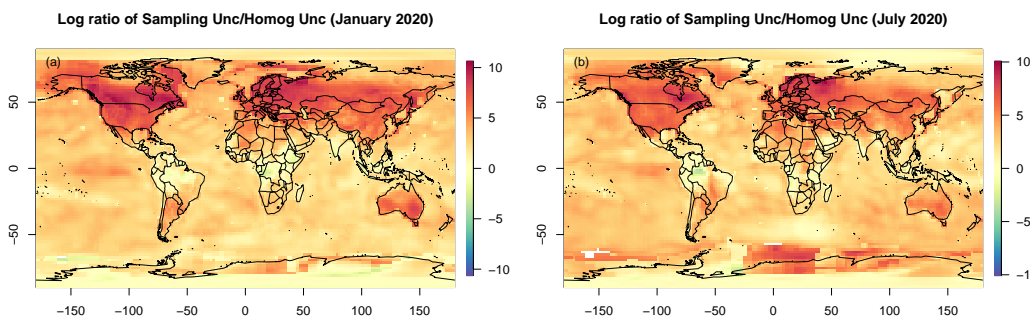


**Figure 7.** The log ratio of sampling and GHCN uncertainty for (a) January 2020 and (b) July 2020. Red regions show where sampling uncertainty dominates and blue regions show where homogenization uncertainty dominates.

341 land surface has greater uncertainty than the ocean at the monthly scale, except during the  
 342 observationally sparse 1940s (Figure 9).

343 The GISTEMP uncertainty ensemble allows easy investigation of the spatial pattern  
 344 of uncertainty at any month in the record. the uncertainty for January 1910, 1940, and 1970  
 345 look broadly similar with generally greater uncertainty over land than the ocean, in regions  
 346 of high temperature variability such as the (particularly winter) mid and high latitudes, and  
 347 in regions with sparse station coverage (Figure 9).

348 The availability of a few uncertainty ensembles allows comparison of the GISTEMP en-  
 349 semble with estimates from HadCRUT5, NOAA GlobalTemp, and DKRZ-DNN (Figure 10).  
 350 Note that each ensemble member from all products have been regridded to the HadCRUT5  
 351  $5^\circ \times 5^\circ$  grid before calculating the standard deviation to facilitate comparison. Comparing  
 352 GISTEMP and HadCRUT5, it is immediately evident that GISTEMP generally estimates  
 353 larger uncertainty over land, particularly in the polar regions. This result is expected as  
 354 HadCRUT5 estimates the sampling and interpolation uncertainty through posterior draws  
 355 from the stationary Gaussian Process used to interpolate data to grid boxes that don't have  
 356 reporting stations. However, this stationary Gaussian Process uses one set of parameters  
 357 fit to the entire globe and, as such, overestimates the signal-to-noise ratio over the  
 358 polar regions where there is both less information of the true spatial field, greater underly-  
 359 ing variance in the true temperature field, and a shorter spatial autocorrelation (Morice et  
 360 al., 2020). By using the empirical estimates of the sampling uncertainty in the GISTEMP  
 361 ensemble, this non-stationarity is avoided and provides a better estimate of the point-wise

362 uncertainty. However, these apparently large differences do not imply large differences in  
363 global annual mean uncertainty (Figure 4) due to the relatively small area of the polar  
364 regions.

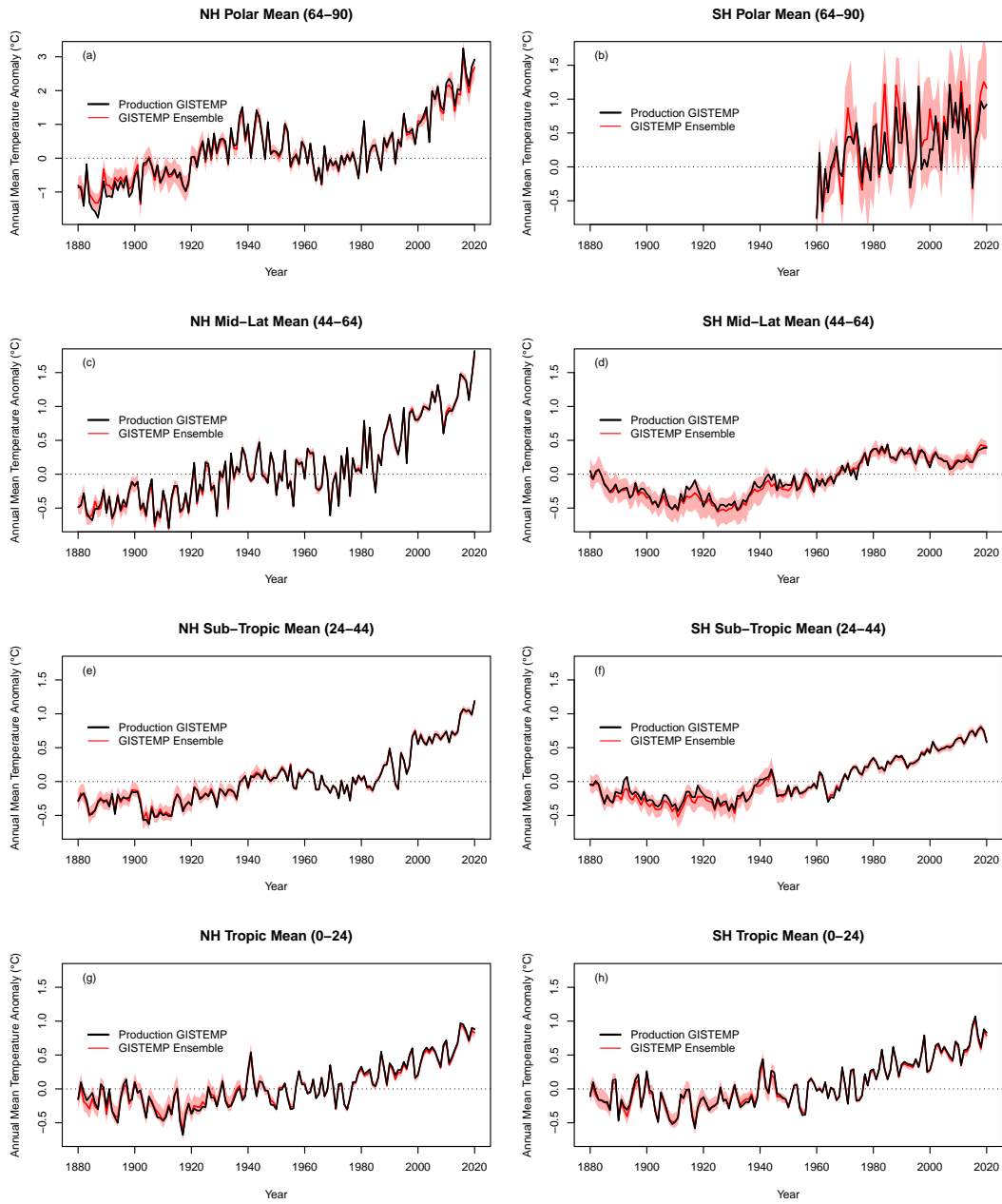


**Figure 8.** A comparison of the annual mean series from the 8 GISTEMP latitudinal bands as calculated from operational GISTEMP and the GISTEMP uncertainty ensemble. The solid red line is the median of the GISTEMP ensemble. Note the different y-scale on the top-left NH Polar plot.

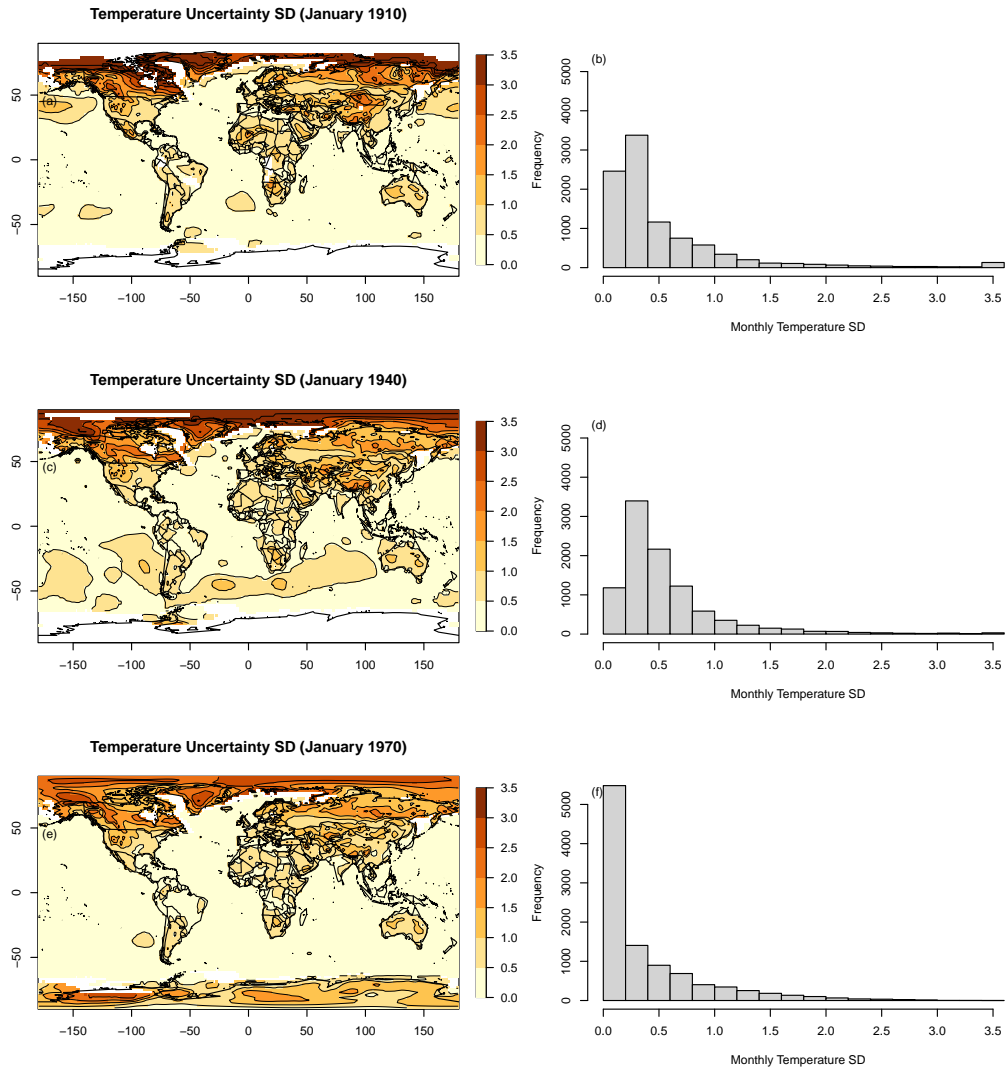


**Figure 9.** The standard deviation of the GISTEMP uncertainty ensemble for three monthly fields. The corresponding histogram to each field is shown to the right. The visualization has been capped at a standard deviation of 3.5 to avoid the very large Antarctic uncertainty dominating the maps.

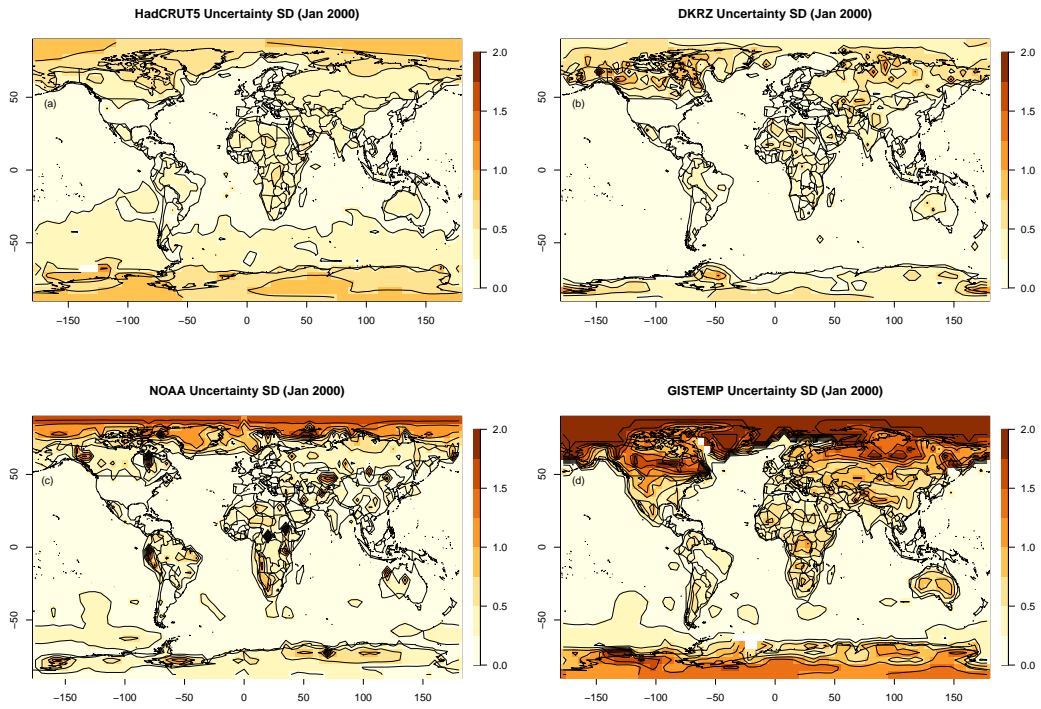


**Figure 10.** Comparison of all global gridded ensemble uncertainty products total uncertainty for January 2000

## 6 Discussion and Conclusions

Here, an uncertainty ensemble for the GISTEMP temperature product has been presented and analyzed. Accounting for all sources of uncertainty at the monthly level increases enables inclusion of historical temperature uncertainty in future studies. The median estimates from the GISTEMP uncertainty ensemble agree very well with operational GISTEMP and the resulting global mean uncertainty agrees with the calculation of Lenssen et al. (2019). This work is a major step forward in the GISTEMP uncertainty model, enabling the inclusion of observational uncertainty in studies on historical global change.

Uncertainty ensembles of gridded products and key time series make including observational uncertainty in subsequent analyses simple. Given an analysis developed using the operational version of GISTEMP, the only additional step is to rerun the analysis on each member of the uncertainty ensemble. Then, results can be summarized using the mean or median estimate of the result of interest as well as empirical confidence intervals. Including uncertainty in surface temperature data is particularly important in regions with high uncertainty such as the polar regions as well as areas with lower forced signals, such as investigations of warming over the eastern tropical pacific and the southern ocean.

This release of an additional uncertainty ensemble form a major global temperature product highlights the need for post-analysis of the available surface temperature uncertainty products. Critical future work includes a comprehensive assessment of the similarities and differences between the 4 temperature ensembles presented here. Such an analysis should investigate both the statistics of the ensembles as well as the results from using these 4 ensembles to answer critical questions about our climate system such as the rate of arctic warming (Rantanen et al., 2022) or the time of emergence of forced signals.

It is the authors' hope that the release of the GISTEMP uncertainty ensemble, alongside the already existing HadCRUT5, NOAA GlobalTemp, and DKRZ DNN uncertainty ensembles, will prompt the community to incorporate observational uncertainty in future studies involving historical surface temperature data whenever possible.

## 7 Open Research

The final gridded and series ensembles are available on the GISTEMP website <https://data.giss.nasa.gov/gistemp/> as well as AWS cloud storage. The operational GISTEMP code used to create the GHCN-ERSST-GISTEMP is also available on the GISTEMP web-

396 site. All of the R analysis code is available on github at [https://github.com/nlenssen/](https://github.com/nlenssen/gistempAWS)  
 397 **gistempAWS**. The full code base, source data and intermediate analyses are available on an  
 398 AWS instance upon request.

### 399 **Acknowledgments**

400 The GISTEMP analysis is funded by the NASA Modeling, Analysis and Prediction program.  
 401 N.L. was also funded from the National Science Foundation Graduate Research Fellowship  
 402 (NSF DGE 16-44869) and the Food and Agriculture Organization (FAO) of the United Na-  
 403 tions. Thanks to Duo Chan, Dorit Hammerling, Boyin Huang, Chris Kadow, Colin Morice,  
 404 Doug Nychka, and Robert Rhode for helpful discussions. Thanks to Hoot Thompson, Gar-  
 405 rison Vaughan, Dan'l Pierce, and Dan Duffy at the NASA Center for Climate Simulation  
 406 (NCCS) for supercomputing and cloud computing support.

### 407 **References**

- 408 Barnes, N., & Jones, D. (2011). Clear Climate Code: Rewriting legacy science software for  
 409 clarity. *IEEE Software*, *28*(6), 36–42. doi: 10.1109/ms.2011.113
- 410 Carleton, T. A., Jina, A., Delgado, M. T., Greenstone, M., Houser, T., Hsiang, S. M., ...  
 411 others (2020). *Valuing the global mortality consequences of climate change accounting*  
 412 *for adaptation costs and benefits* (Tech. Rep.). Cambridge, MA: National Bureau of  
 413 Economic Research.
- 414 Chan, D., Kent, E. C., Berry, D. I., & Huybers, P. (2019). Correcting datasets leads to  
 415 more homogeneous early-twentieth-century sea surface warming. *Nature*, *571*(7765),  
 416 393–397.
- 417 Cowtan, K., Jacobs, P., Thorne, P., & Wilkinson, R. (2018, 07). Statistical analysis of  
 418 coverage error in simple global temperature estimators. *Dynamics and Statistics of the*  
 419 *Climate System*, *3*(1), dzy003. Retrieved from [https://doi.org/10.1093/climsys/](https://doi.org/10.1093/climsys/dzy003)  
 420 [dzy003](https://doi.org/10.1093/climsys/dzy003) doi: 10.1093/climsys/dzy003
- 421 Danabasoglu, G., Lamarque, J.-F., Bacmeister, J., Bailey, D., DuVivier, A., Edwards, J.,  
 422 ... others (2020). The community earth system model version 2 (cesm2). *Journal of*  
 423 *Advances in Modeling Earth Systems*, *12*(2), e2019MS001916.
- 424 Hansen, J., & Lebedeff, S. (1987). Global trends of measured surface air temperature. *Jour-*  
 425 *nal of Geophysical Research: Atmospheres*, *92*(D11), 13345–13372. Retrieved from  
 426 <http://dx.doi.org/10.1029/JD092iD11p13345> doi: 10.1029/JD092iD11p13345

- 427 Hansen, J., Ruedy, R., Sato, M., & Lo, K. (2010). Global surface temperature  
428 change. *Reviews of Geophysics*, *48*(4). Retrieved from [http://dx.doi.org/10.1029/](http://dx.doi.org/10.1029/2010RG000345)  
429 [2010RG000345](http://dx.doi.org/10.1029/2010RG000345) (RG4004) doi: 10.1029/2010RG000345
- 430 Hausfather, Z., Drake, H. F., Abbott, T., & Schmidt, G. A. (2020). Evaluating the per-  
431 formance of past climate model projections. *Geophysical Research Letters*, *47*(1),  
432 e2019GL085378.
- 433 Hausfather, Z., Menne, M. J., Williams, C. N., Masters, T., Broberg, R., & Jones, D.  
434 (2013). Quantifying the effect of urbanization on u.s. historical climatology network  
435 temperature records. *Journal of Geophysical Research: Atmospheres*, *118*(2), 481–494.  
436 doi: 10.1029/2012jd018509
- 437 Held, I., Guo, H., Adcroft, A., Dunne, J., Horowitz, L., Krasting, J., ... others (2019).  
438 Structure and performance of gfdl’s cm4. 0 climate model. *Journal of Advances in*  
439 *Modeling Earth Systems*, *11*(11), 3691–3727.
- 440 Hersbach, H., Bell, B., Berrisford, P., Hirahara, S., Horányi, A., Muñoz-Sabater, J., ...  
441 Thépaut, J.-N. (2020). The ERA5 global reanalysis. *Quarterly Journal of the*  
442 *Royal Meteorological Society*, *146*(730), 1999–2049. Retrieved from [https://rmets](https://rmets.onlinelibrary.wiley.com/doi/abs/10.1002/qj.3803)  
443 [.onlinelibrary.wiley.com/doi/abs/10.1002/qj.3803](https://rmets.onlinelibrary.wiley.com/doi/abs/10.1002/qj.3803) doi: [https://doi.org/10](https://doi.org/10.1002/qj.3803)  
444 [.1002/qj.3803](https://doi.org/10.1002/qj.3803)
- 445 Huang, B., Menne, M. J., Boyer, T., Freeman, E., Gleason, B. E., Lawrimore, J. H., ...  
446 Zhang, H.-M. (2020). Uncertainty estimates for sea surface temperature and land  
447 surface air temperature in noaaglobaltemp version 5. *Journal of Climate*, *33*(4), 1351  
448 - 1379. Retrieved from [https://journals.ametsoc.org/view/journals/clim/33/](https://journals.ametsoc.org/view/journals/clim/33/4/jcli-d-19-0395.1.xml)  
449 [4/jcli-d-19-0395.1.xml](https://journals.ametsoc.org/view/journals/clim/33/4/jcli-d-19-0395.1.xml) doi: 10.1175/JCLI-D-19-0395.1
- 450 Huang, B., Thorne, P. W., Banzon, V. F., Boyer, T., Chepurin, G., Lawrimore, J. H.,  
451 ... Zhang, H.-M. (2017). Extended reconstructed sea surface temperature, version 5  
452 (ersstv5): Upgrades, validations, and intercomparisons. *Journal of Climate*, *30*(20),  
453 8179 - 8205. Retrieved from [https://journals.ametsoc.org/view/journals/clim/](https://journals.ametsoc.org/view/journals/clim/30/20/jcli-d-16-0836.1.xml)  
454 [30/20/jcli-d-16-0836.1.xml](https://journals.ametsoc.org/view/journals/clim/30/20/jcli-d-16-0836.1.xml) doi: 10.1175/JCLI-D-16-0836.1
- 455 Huang, B., Thorne, P. W., Smith, T. M., Liu, W., Lawrimore, J., Banzon, V. F., ... Menne,  
456 M. (2016). Further exploring and quantifying uncertainties for extended reconstructed  
457 sea surface temperature (ersst) version 4 (v4). *Journal of Climate*, *29*(9), 3119–3142.
- 458 Kadow, C., Hall, D. M., & Ulbrich, U. (2020). Artificial intelligence reconstructs missing  
459 climate information. *Nature Geoscience*, *13*(6), 408–413.

- 460 Lensen, N. J. L., Schmidt, G. A., Hansen, J. E., Menne, M. J., Persin, A., Ruedy, R.,  
 461 & Zyss, D. (2019). Improvements in the GISTEMP uncertainty model. *Journal of*  
 462 *Geophysical Research: Atmospheres*, *124*(12), 6307-6326. Retrieved from [https://](https://agupubs.onlinelibrary.wiley.com/doi/abs/10.1029/2018JD029522)  
 463 [agupubs.onlinelibrary.wiley.com/doi/abs/10.1029/2018JD029522](https://agupubs.onlinelibrary.wiley.com/doi/abs/10.1029/2018JD029522) doi: 10  
 464 .1029/2018JD029522
- 465 Liu, W., Huang, B., Thorne, P. W., Banzon, V. F., Zhang, H.-M., Freeman, E., ...  
 466 Woodruff, S. D. (2015). Extended reconstructed sea surface temperature version  
 467 4 (ersst.v4): Part ii. parametric and structural uncertainty estimations. *Journal of*  
 468 *Climate*, *28*(3), 931 - 951. Retrieved from [https://journals.ametsoc.org/view/](https://journals.ametsoc.org/view/journals/clim/28/3/jcli-d-14-00007.1.xml)  
 469 [journals/clim/28/3/jcli-d-14-00007.1.xml](https://journals.ametsoc.org/view/journals/clim/28/3/jcli-d-14-00007.1.xml) doi: 10.1175/JCLI-D-14-00007.1
- 470 Menne, M. J., Williams, C. N., Gleason, B. E., Rennie, J. J., & Lawrimore, J. H. (2018, sep).  
 471 The Global Historical Climatology Network monthly temperature dataset, version 4.  
 472 *Journal of Climate*. Retrieved from <https://doi.org/10.1175/jcli-d-18-0094.1>  
 473 doi: 10.1175/jcli-d-18-0094.1
- 474 Morice, C. P., Kennedy, J. J., Rayner, N. A., & Jones, P. D. (2012, 4). Quantifying  
 475 uncertainties in global and regional temperature change using an ensemble of observa-  
 476 tional estimates: The HadCRUT4 data set. *Journal of Geophysical Research: Atmo-*  
 477 *spheres*, *117*(D8). Retrieved from <http://doi.wiley.com/10.1029/2011JD017187>  
 478 doi: 10.1029/2011JD017187
- 479 Morice, C. P., Kennedy, J. J., Rayner, N. A., Winn, J. P., Hogan, E., Killick, R. E., ...  
 480 Simpson, I. R. (2020). An updated assessment of near-surface temperature change  
 481 from 1850: the HadCRUT5 dataset. *Journal of Geophysical Research*.
- 482 Myhre, G., Alterskjær, K., Stjern, C. W., Hodnebrog, Ø., Marelle, L., Samset, B. H., ...  
 483 others (2019). Frequency of extreme precipitation increases extensively with event  
 484 rareness under global warming. *Scientific reports*, *9*(1), 1-10.
- 485 Notz, D., & SIMIP Community. (2020). Arctic sea ice in cmip6. *Geophysical Research*  
 486 *Letters*, *47*(10), e2019GL086749.
- 487 R Core Team. (2020). R: A language and environment for statistical computing [Computer  
 488 software manual]. Vienna, Austria. Retrieved from <https://www.R-project.org/>
- 489 Rantanen, M., Karpechko, A. Y., Lipponen, A., Nordling, K., Hyvärinen, O., Ruosteenoja,  
 490 K., ... Laaksonen, A. (2022). The arctic has warmed nearly four times faster than  
 491 the globe since 1979. *Communications Earth & Environment*, *3*(1), 168.
- 492 Rohde, R. A., & Hausfather, Z. (2020). The berkeley earth land/ocean temperature

493 record. *Earth System Science Data*, 12(4), 3469–3479. Retrieved from <https://>  
494 [essd.copernicus.org/articles/12/3469/2020/](https://essd.copernicus.org/articles/12/3469/2020/) doi: 10.5194/essd-12-3469-2020  
495 Swart, N. C., Cole, J. N., Kharin, V. V., Lazare, M., Scinocca, J. F., Gillett, N. P., . . . others  
496 (2019). The canadian earth system model version 5 (canesm5. 0.3). *Geoscientific Model*  
497 *Development*, 12(11), 4823–4873.  
498 Tokarska, K. B., Stolpe, M. B., Sippel, S., Fischer, E. M., Smith, C. J., Lehner, F., &  
499 Knutti, R. (2020). Past warming trend constrains future warming in cmip6 models.  
500 *Science advances*, 6(12), eaaz9549.

Figure 1.

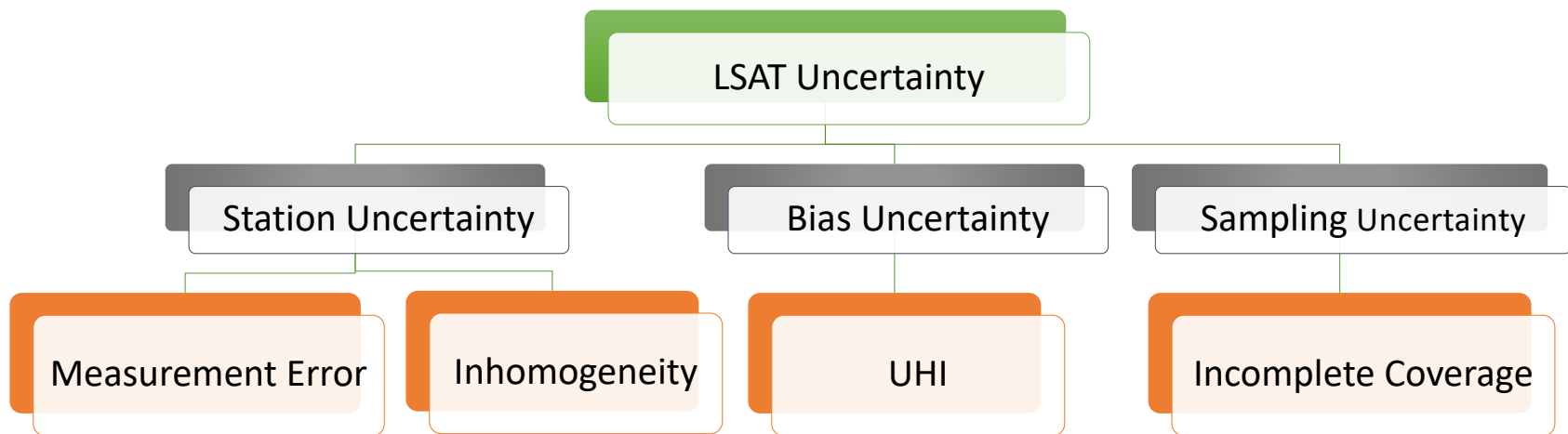


Figure 2.

NOAA FTP Server: ftp.ncdc.noaa.gov

- Python
- R
- Discover/Shell
- NetCDF
- Text File

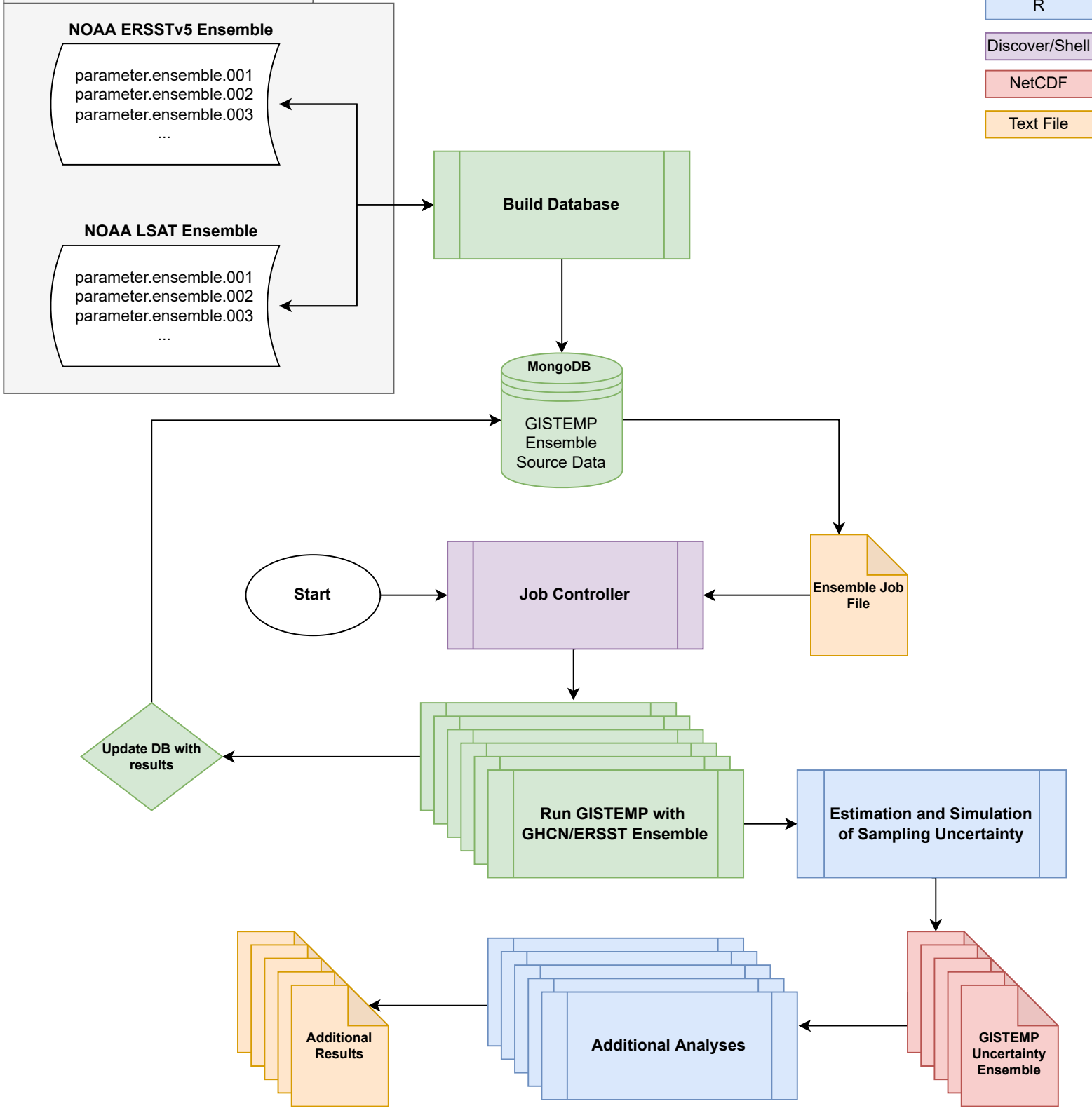
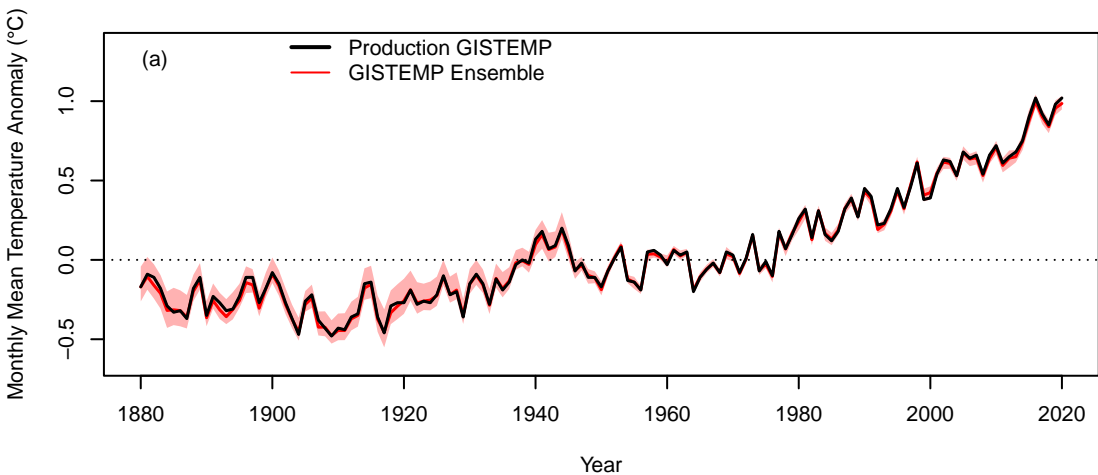
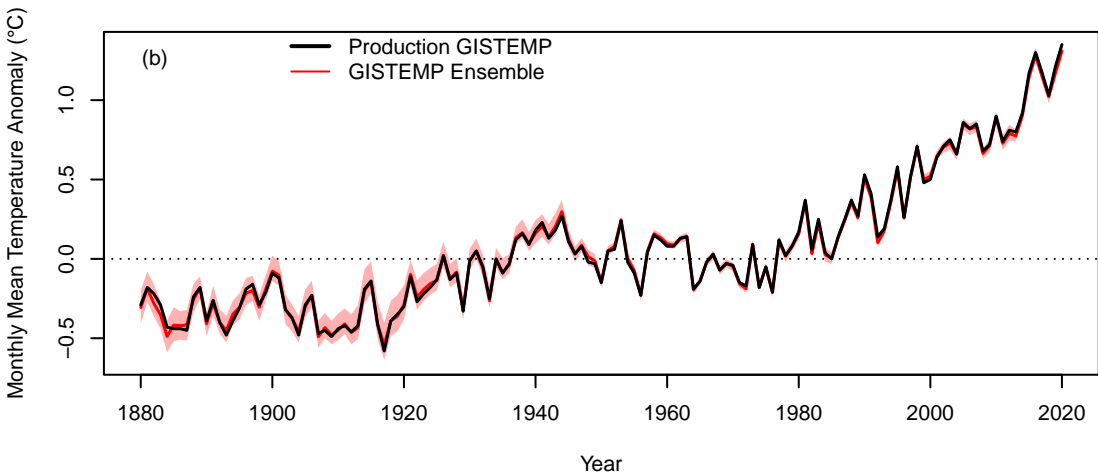


Figure 3.

### Global Mean



### Northern Hemisphere Mean



### Southern Hemisphere Mean

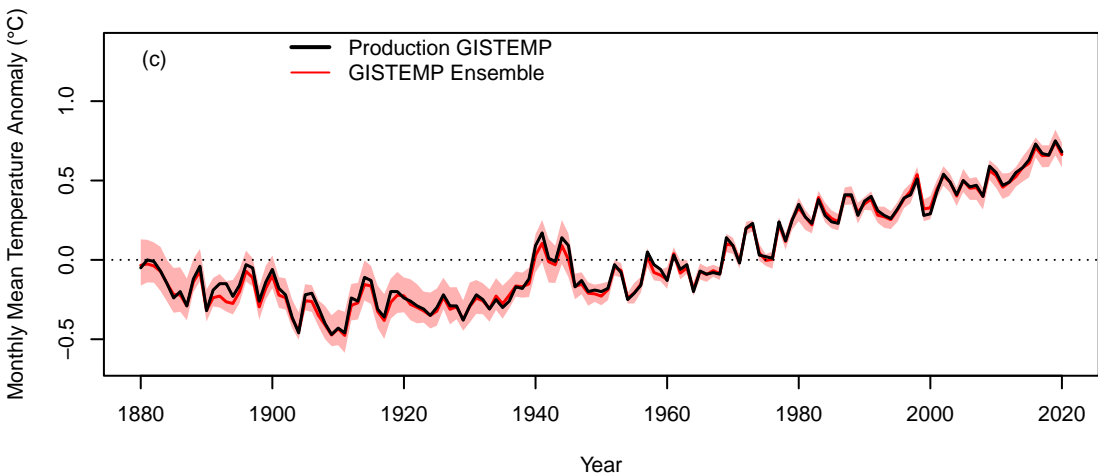


Figure 4.

## Comparison of Global Annual Uncertainty Estimates

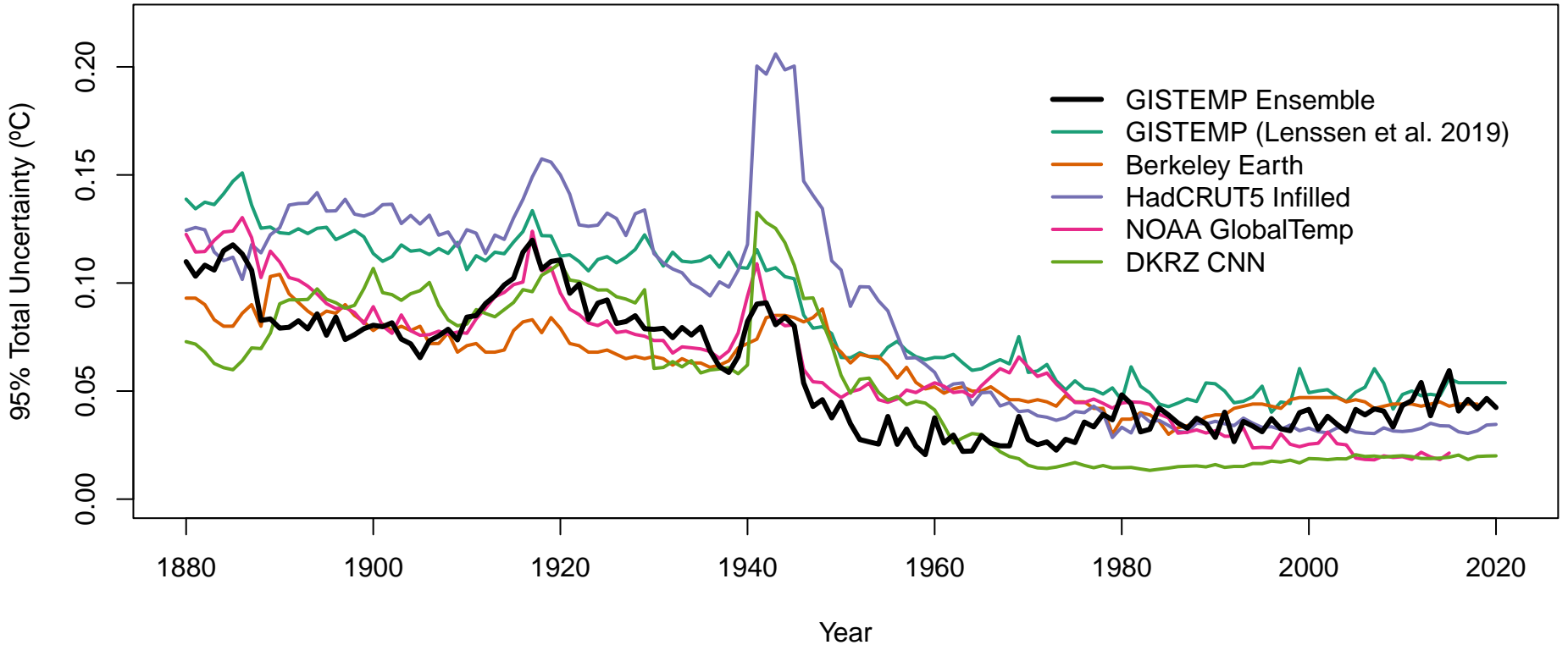
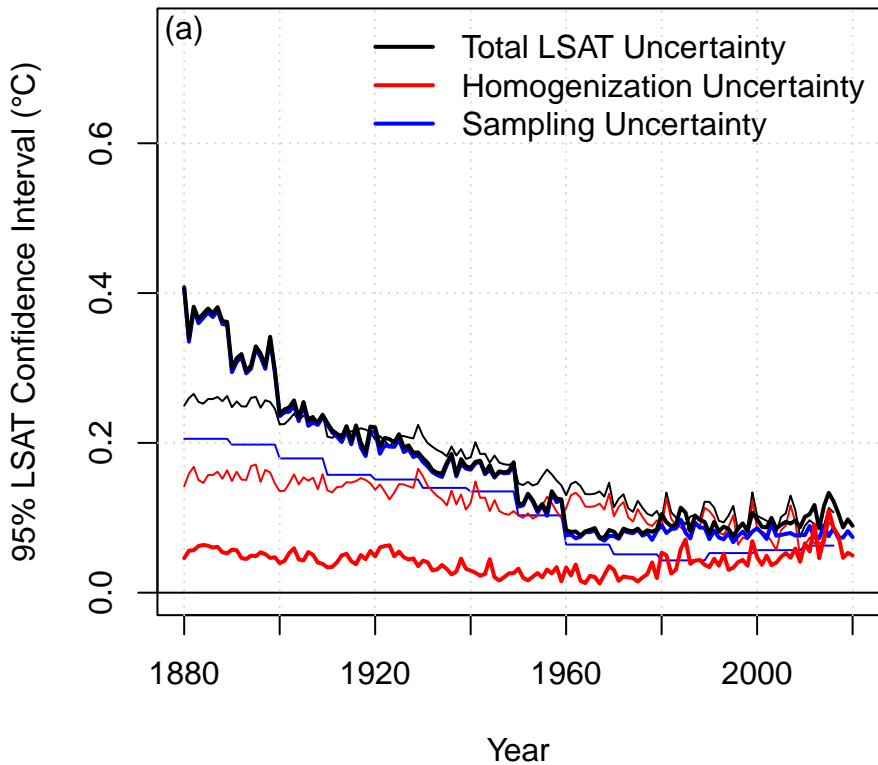


Figure 5.

## LSAT Uncertainty Decomposition



## Difference from Lenssen et al. (2019)

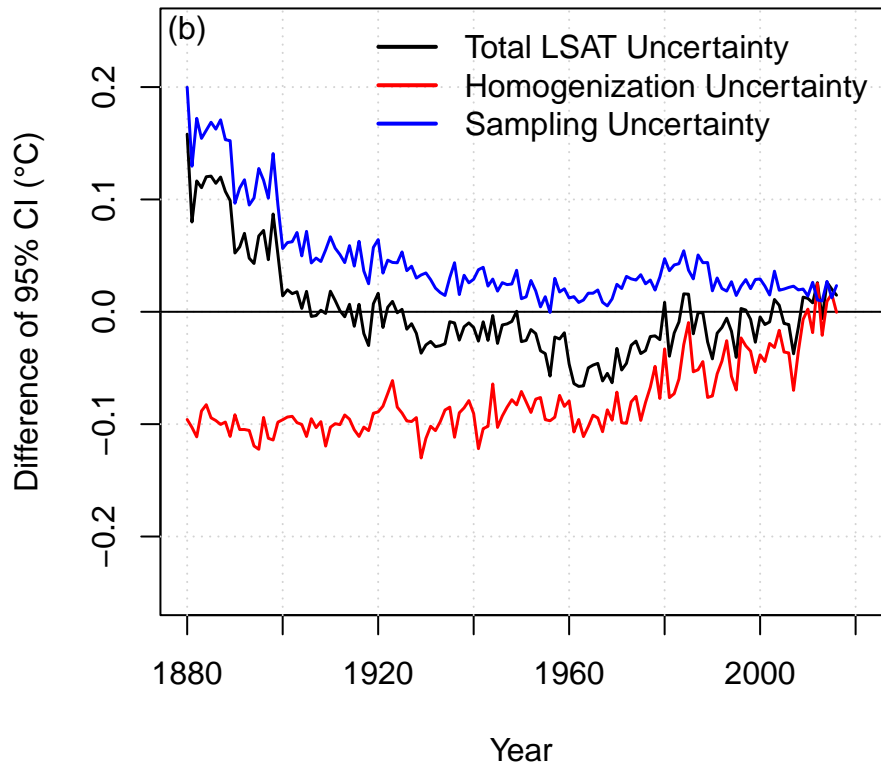
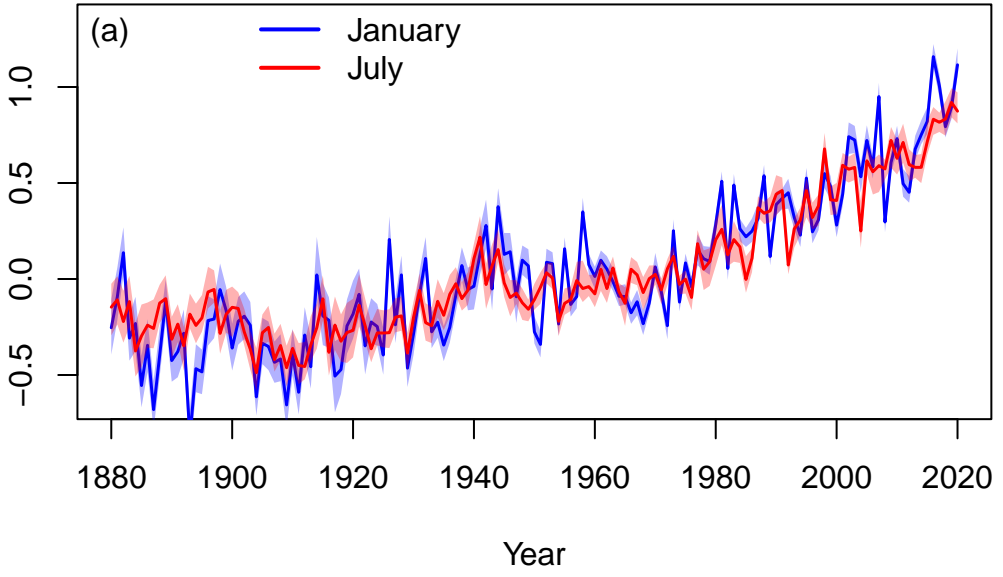


Figure 6.

# Monthly Global Mean Anomaly

Monthly Mean Temperature Anomaly (°C)



# Global Mean Temperature (ERA5 Seasonal Cycle)

Monthly Anomaly Relative to Annual Mean (°C)

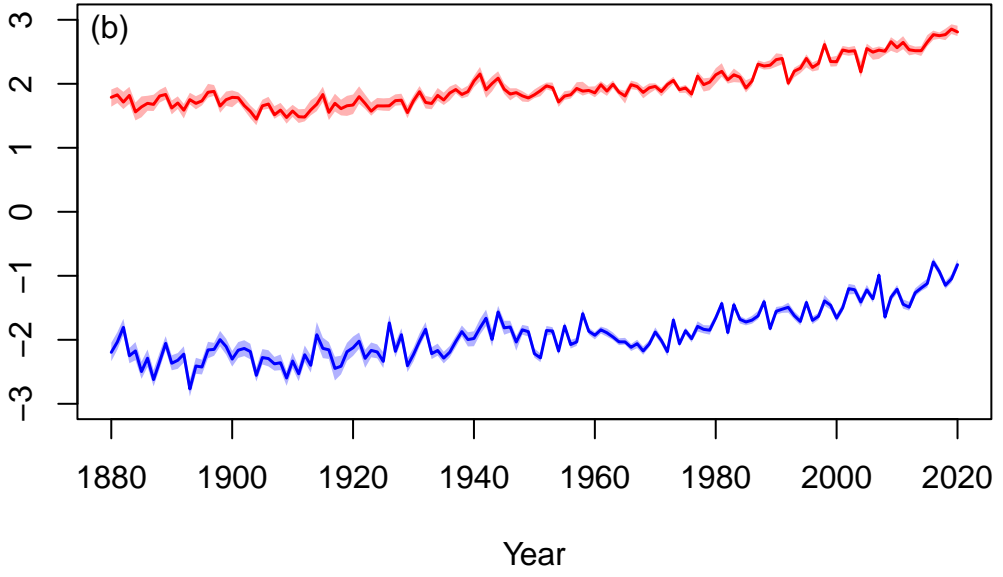
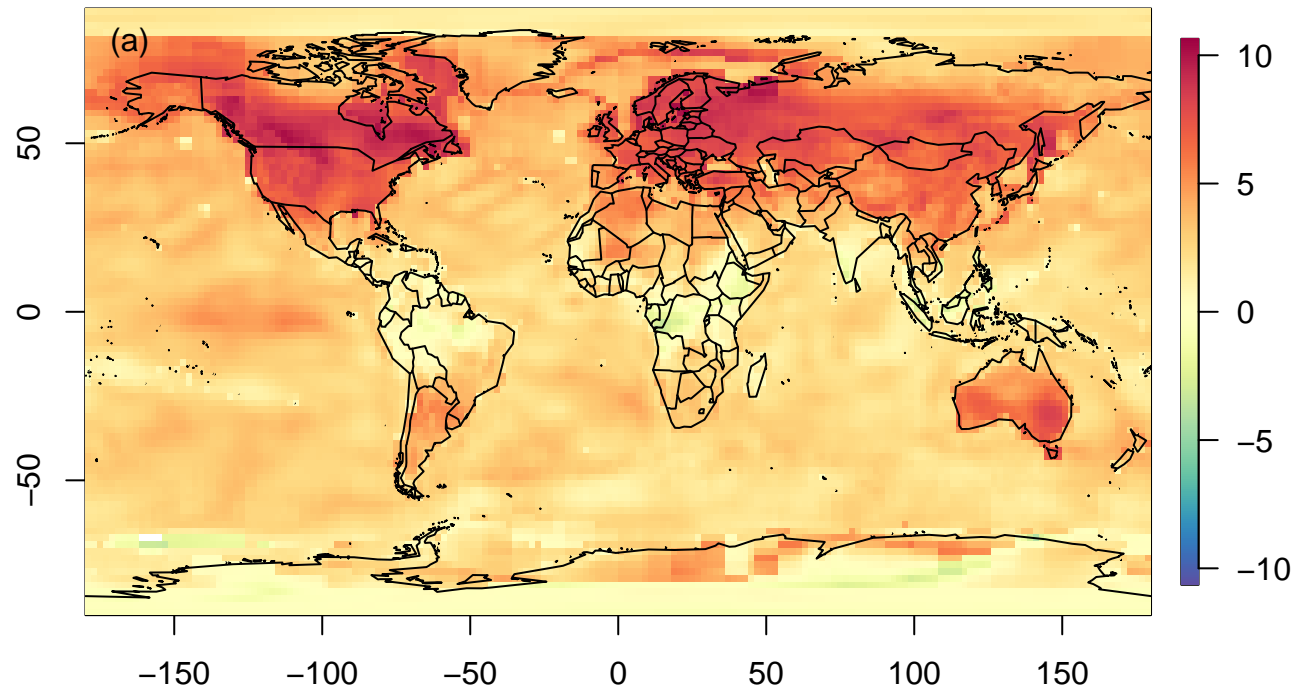


Figure 7.

Log ratio of Sampling Unc/Homog Unc (January 2020)



Log ratio of Sampling Unc/Homog Unc (July 2020)

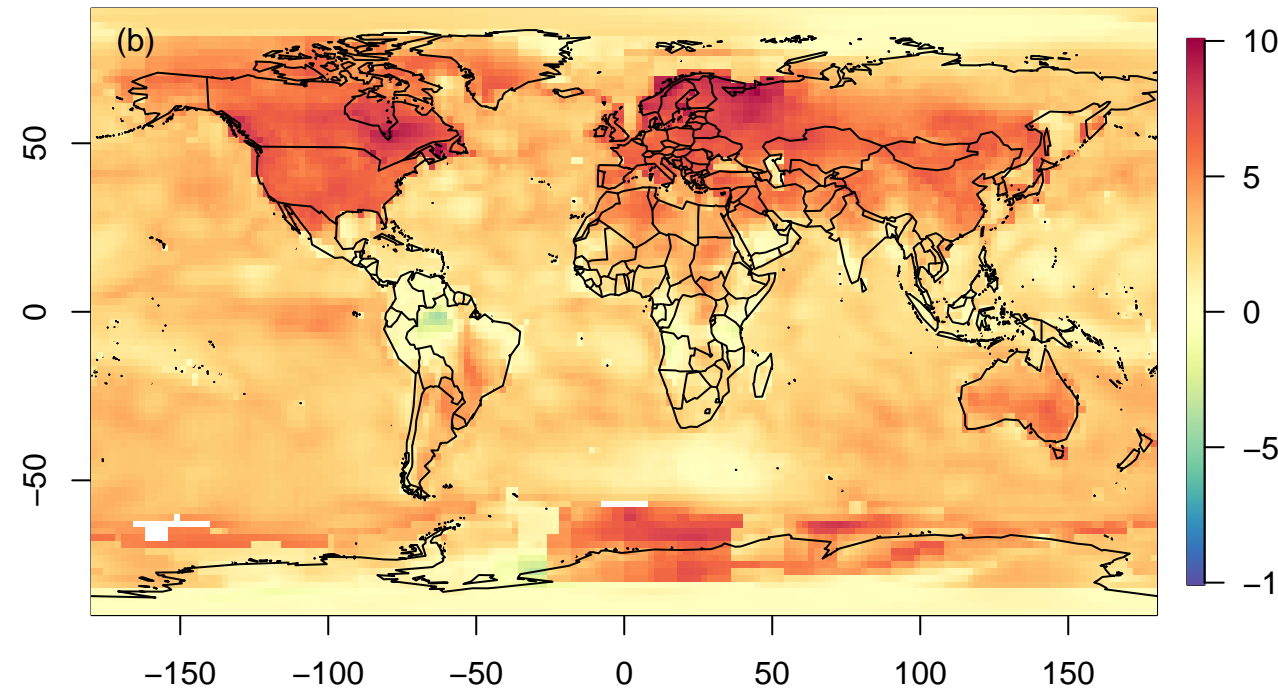


Figure 8.

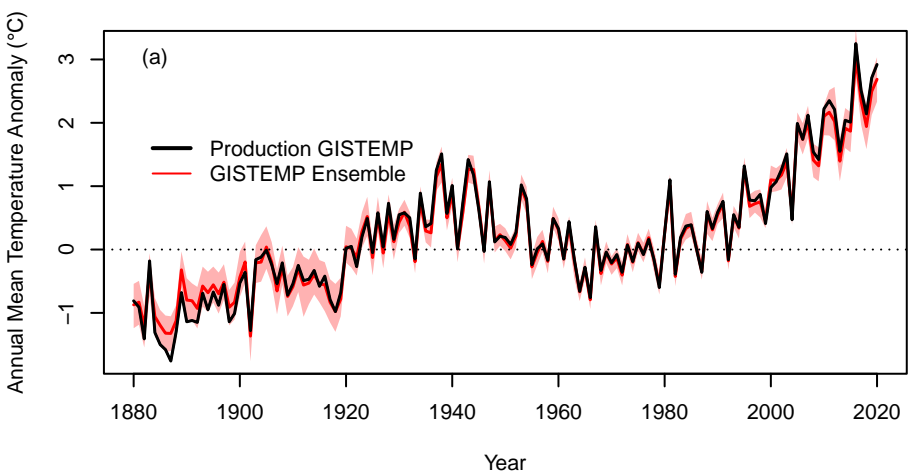
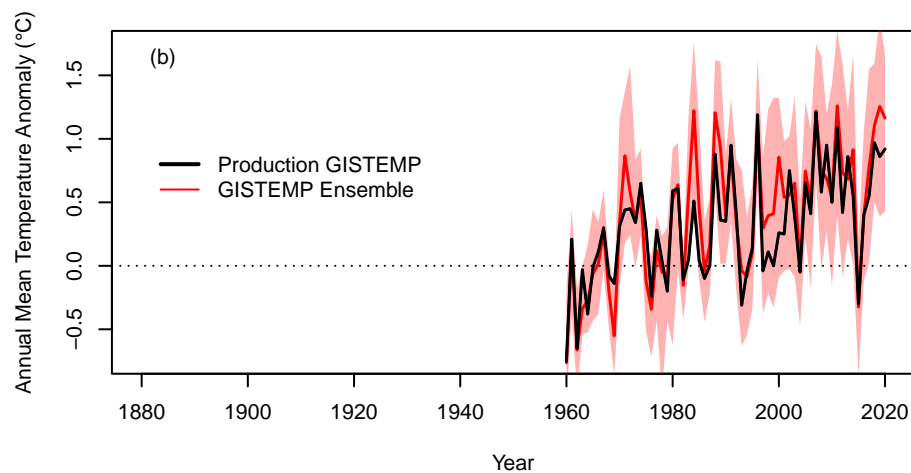
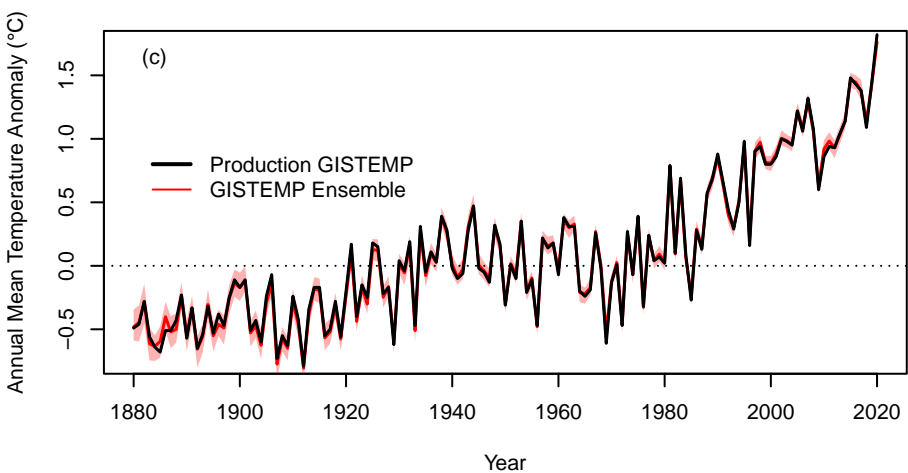
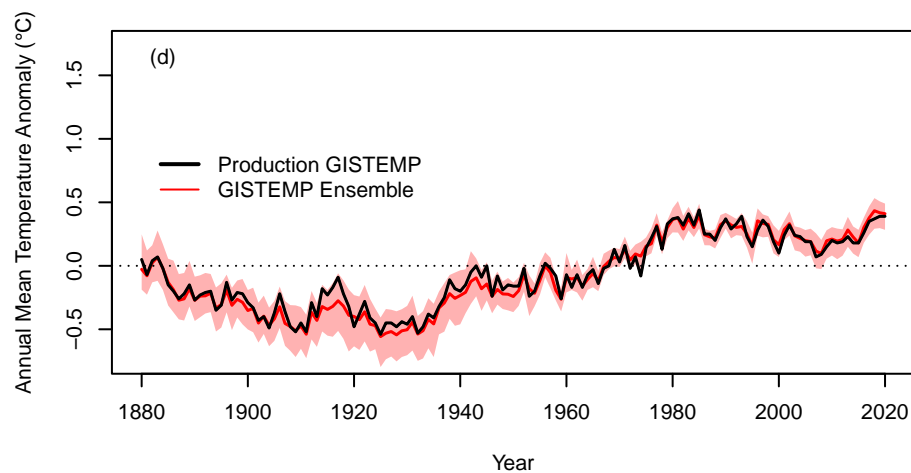
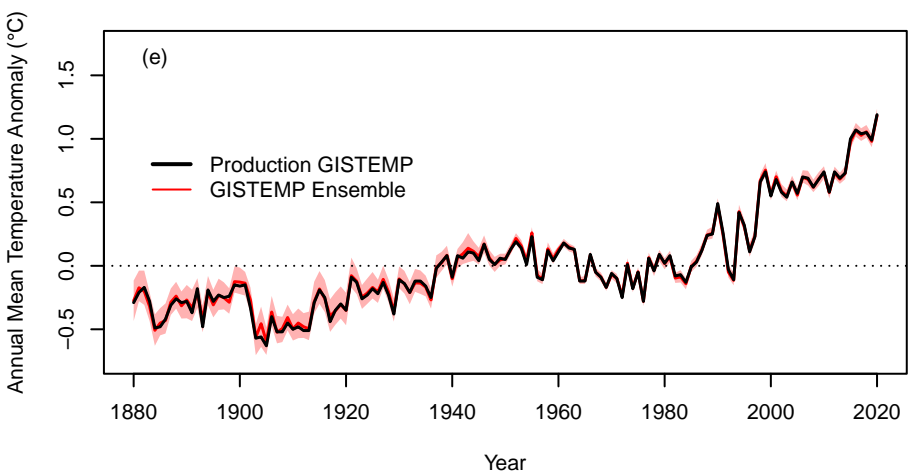
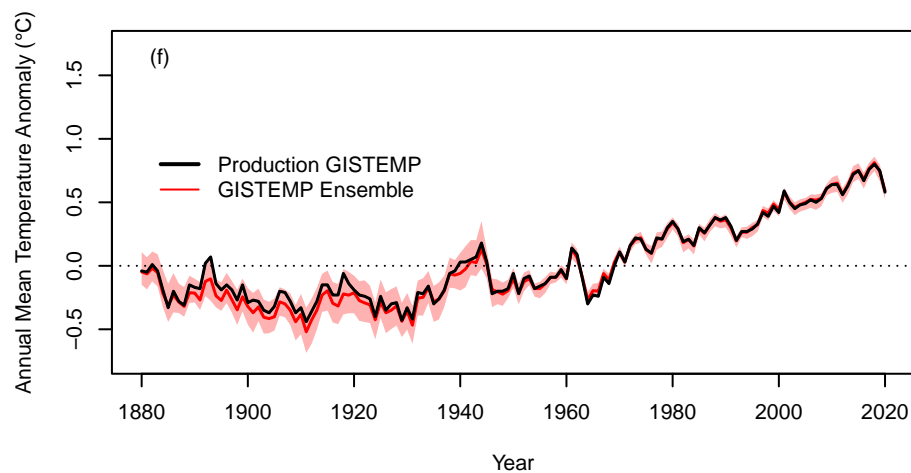
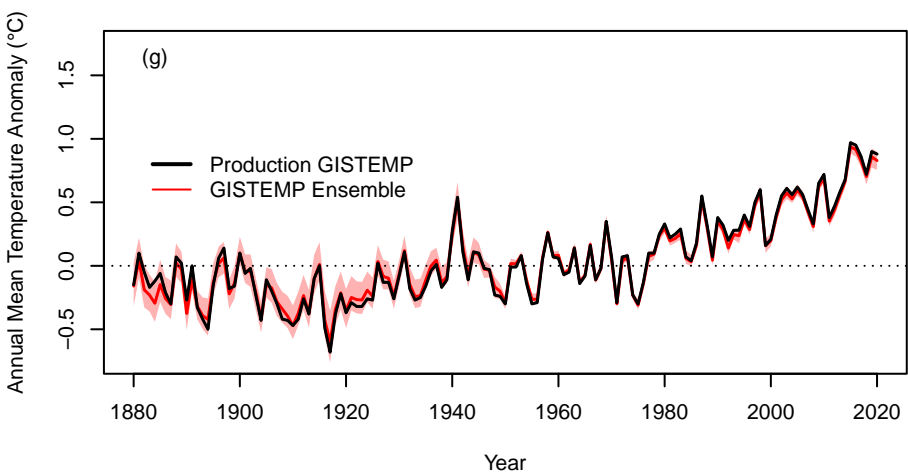
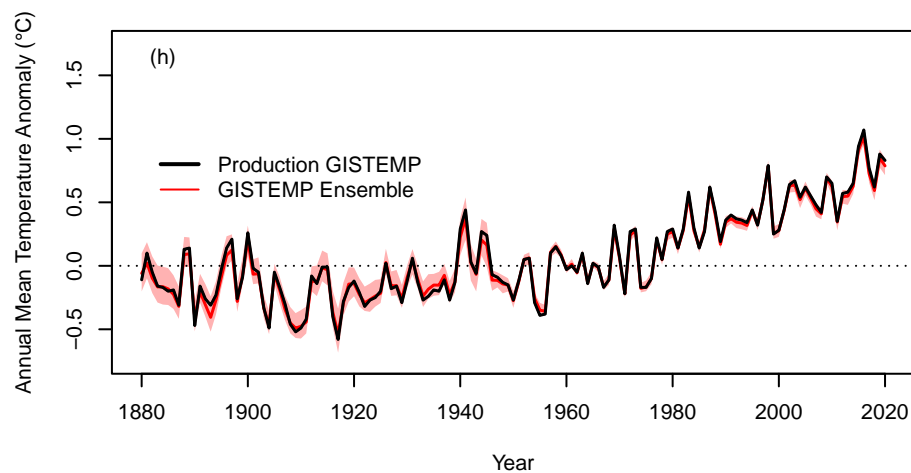
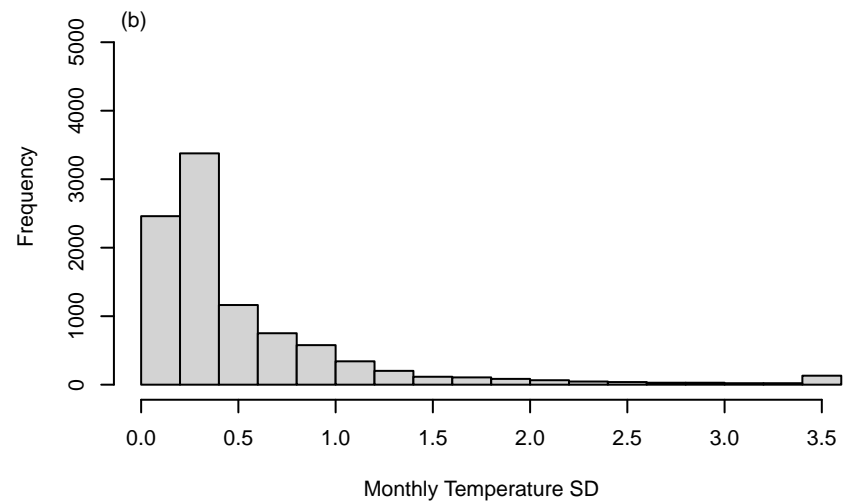
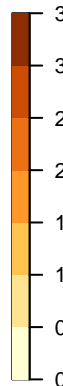
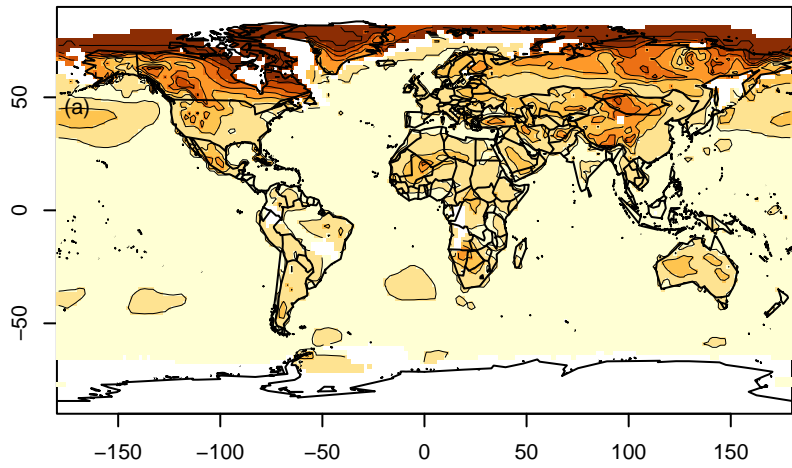
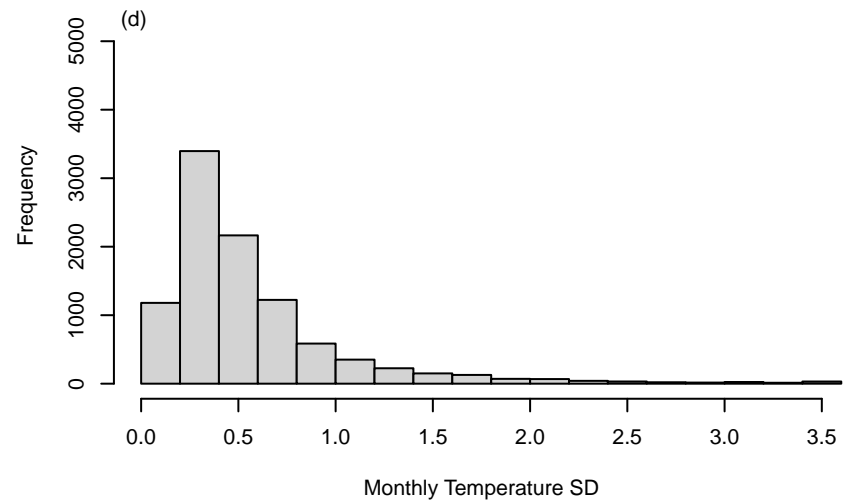
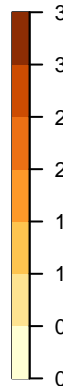
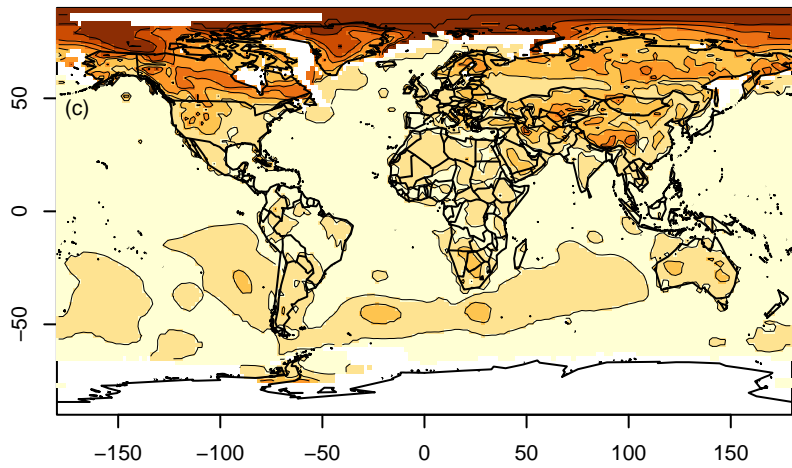
**NH Polar Mean (64–90)****SH Polar Mean (64–90)****NH Mid-Lat Mean (44–64)****SH Mid-Lat Mean (44–64)****NH Sub-Tropic Mean (24–44)****SH Sub-Tropic Mean (24–44)****NH Tropic Mean (0–24)****SH Tropic Mean (0–24)**

Figure 9.

Temperature Uncertainty SD (January 1910)



Temperature Uncertainty SD (January 1940)



Temperature Uncertainty SD (January 1970)

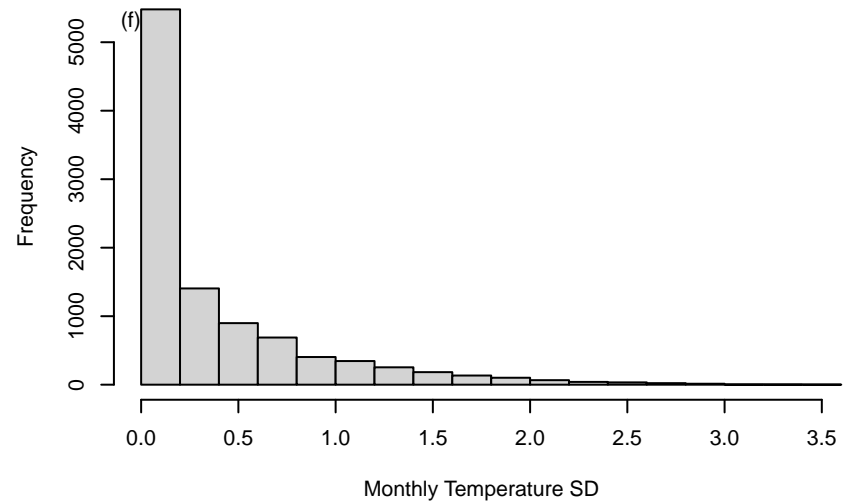
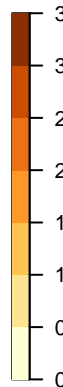
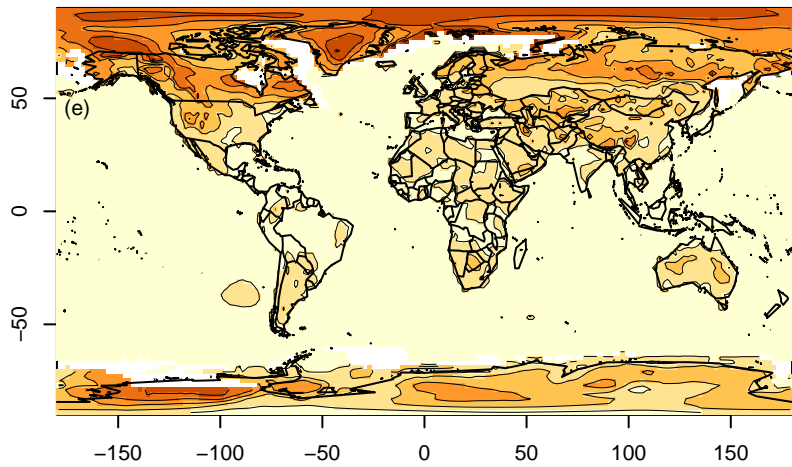
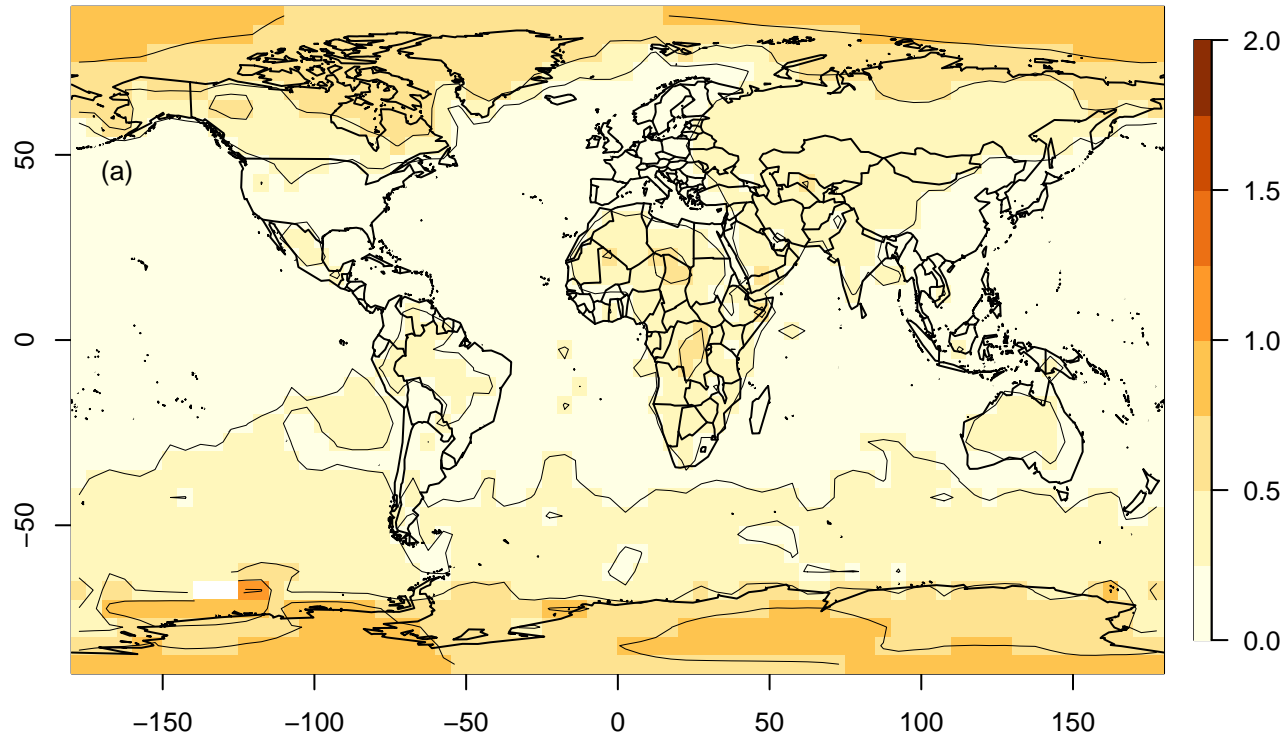
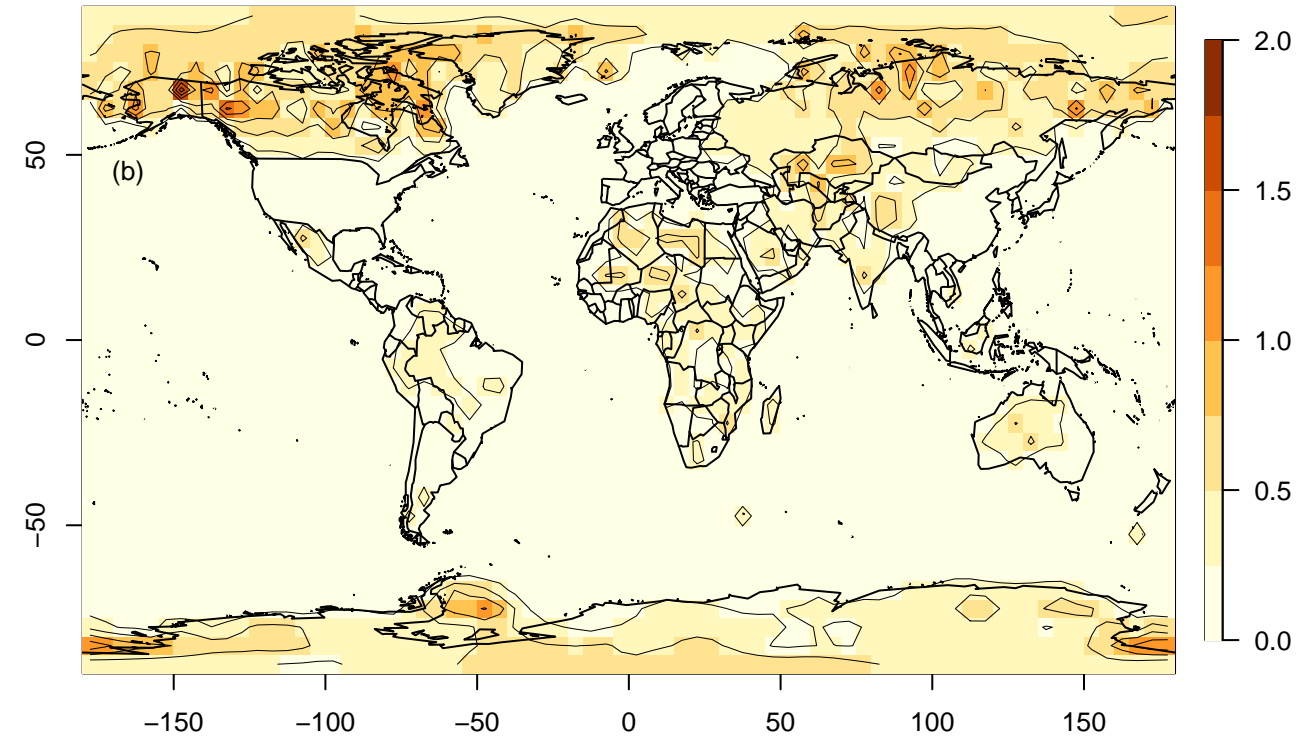


Figure 10.

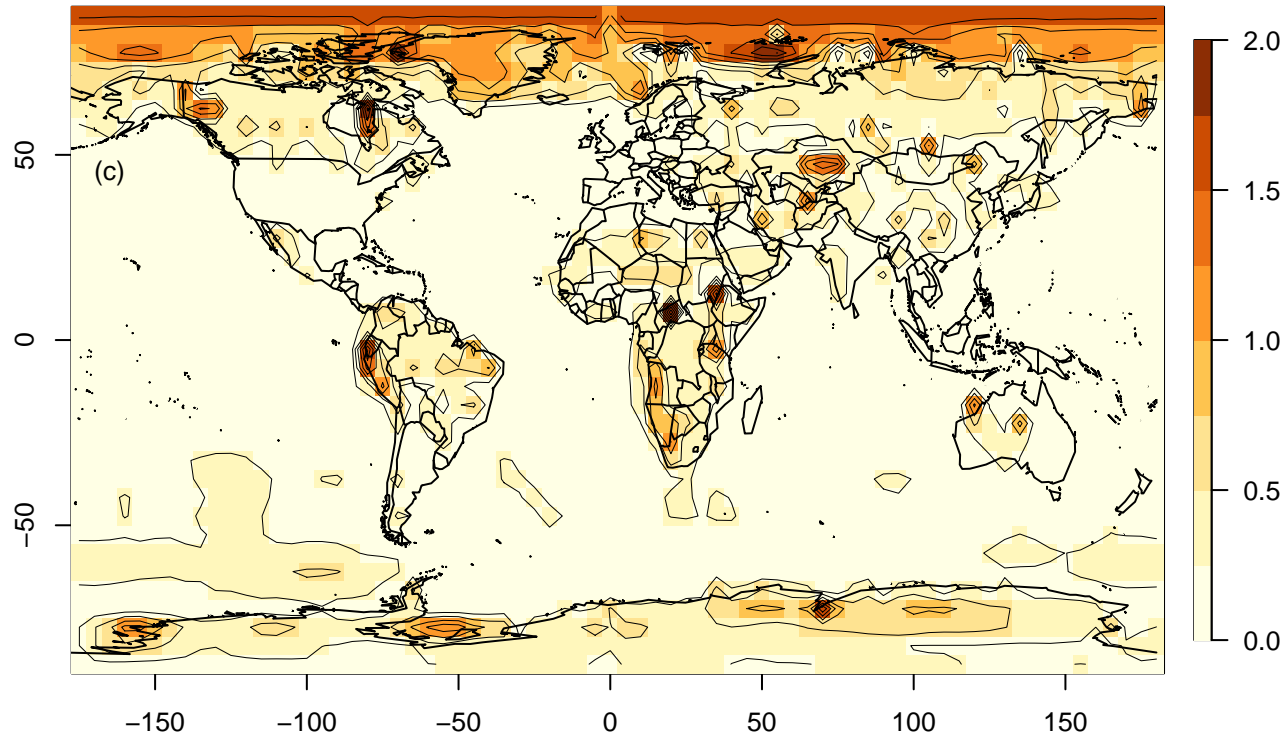
**HadCRUT5 Uncertainty SD (Jan 2000)**



**DKRZ Uncertainty SD (Jan 2000)**



**NOAA Uncertainty SD (Jan 2000)**



**GISTEMP Uncertainty SD (Jan 2000)**

